Atmos. Meas. Tech., 9, 3491–3512, 2016
www.atmos-meas-tech.net/9/3491/2016/
doi:10.5194/amt-9-3491-2016
© Author(s) 2016. CC Attribution 3.0 License.

Atmospheric Measurement Techniques
Open Access
EGU

Bias corrections of GOSAT SWIR XCO_2 and XCH_4 with TCCON data and their evaluation using aircraft measurement data

Makoto Inoue[1,a], Isamu Morino[1], Osamu Uchino[1], Takahiro Nakatsuru[1], Yukio Yoshida[1], Tatsuya Yokota[1], Debra Wunch[2,b], Paul O. Wennberg[2], Coleen M. Roehl[2], David W. T. Griffith[3], Voltaire A. Velazco[3], Nicholas M. Deutscher[3,4], Thorsten Warneke[4], Justus Notholt[4], John Robinson[5], Vanessa Sherlock[5,c], Frank Hase[6], Thomas Blumenstock[6], Markus Rettinger[7], Ralf Sussmann[7], Esko Kyrö[8], Rigel Kivi[8], Kei Shiomi[9], Shuji Kawakami[9], Martine De Mazière[10], Sabrina G. Arnold[11], Dietrich G. Feist[11], Erica A. Barrow[12], James Barney[12], Manvendra Dubey[13], Matthias Schneider[6], Laura T. Iraci[14], James R. Podolske[14], Patrick W. Hillyard[14,15], Toshinobu Machida[1], Yousuke Sawa[16], Kazuhiro Tsuboi[16], Hidekazu Matsueda[16], Colm Sweeney[17], Pieter P. Tans[17], Arlyn E. Andrews[17], Sebastien C. Biraud[18], Yukio Fukuyama[19], Jasna V. Pittman[20], Eric A. Kort[21,2,d], and Tomoaki Tanaka[1,9,e]

[1]National Institute for Environmental Studies (NIES), Tsukuba, Japan
[2]California Institute for Technology, Pasadena, CA, USA
[3]Centre for Atmospheric Chemistry, University of Wollongong, New South Wales, Australia
[4]Institute of Environmental Physics, University of Bremen, Bremen, Germany
[5]National Institute of Water and Atmospheric Research, Lauder, New Zealand
[6]IMK-ASF, Karlsruhe Institute of Technology, Karlsruhe, Germany
[7]IMK-IFU, Karlsruhe Institute of Technology, Garmisch-Partenkirchen, Germany
[8]Arctic Research Centre, Finnish Meteorological Institute (FMI), Sodankylä, Finland
[9]Japan Aerospace Exploration Agency (JAXA), Tsukuba, Japan
[10]Belgian Institute for Space Aeronomy (IASB-BIRA), Brussels, Belgium
[11]Max Planck Institute for Biogeochemistry (MPI-BGC), Jena, Germany
[12]Ivy Tech Community College of Indiana, Indianapolis, IN, USA
[13]Los Alamos National Laboratory, Los Alamos, NM, USA
[14]NASA Ames Research Center, Moffett Field, CA, USA
[15]Bay Area Environmental Research Institute, Petaluma, CA, USA
[16]Meteorological Research Institute (MRI), Tsukuba, Japan
[17]National Oceanic and Atmospheric Administration (NOAA), Boulder, CO, USA
[18]Lawrence Berkeley National Laboratory (LBNL), Berkeley, CA, USA
[19]Japan Meteorological Agency, Tokyo, Japan
[20]Department of Earth and Planetary Sciences, Harvard University, Cambridge, MA, USA
[21]Jet Propulsion Laboratory, Pasadena, CA, USA
[a]now at: Department of Biological Environment, Akita Prefectural University, Akita, Japan
[b]now at: Department of Physics, University of Toronto, Toronto, Canada
[c]now at: Laboratoire de Météorologie Dynamique, Palaiseau, France
[d]now at: Department of Atmospheric, Oceanic and Space Sciences, University of Michigan, Ann Arbor, MI, USA
[e]now at: NASA Ames Research Center, Moffett Field, CA, USA

Correspondence to: Makoto Inoue (makoto@akita-pu.ac.jp)

Received: 25 November 2015 – Published in Atmos. Meas. Tech. Discuss.: 18 January 2016
Revised: 24 June 2016 – Accepted: 29 June 2016 – Published: 1 August 2016

Published by Copernicus Publications on behalf of the European Geosciences Union.

Abstract. We describe a method for removing systematic biases of column-averaged dry air mole fractions of CO_2 (XCO_2) and CH_4 (XCH_4) derived from short-wavelength infrared (SWIR) spectra of the Greenhouse gases Observing SATellite (GOSAT). We conduct correlation analyses between the GOSAT biases and simultaneously retrieved auxiliary parameters. We use these correlations to bias correct the GOSAT data, removing these spurious correlations. Data from the Total Carbon Column Observing Network (TCCON) were used as reference values for this regression analysis. To evaluate the effectiveness of this correction method, the uncorrected/corrected GOSAT data were compared to independent XCO_2 and XCH_4 data derived from aircraft measurements taken for the Comprehensive Observation Network for TRace gases by AIrLiner (CONTRAIL) project, the National Oceanic and Atmospheric Administration (NOAA), the US Department of Energy (DOE), the National Institute for Environmental Studies (NIES), the Japan Meteorological Agency (JMA), the HIAPER Pole-to-Pole observations (HIPPO) program, and the GOSAT validation aircraft observation campaign over Japan. These comparisons demonstrate that the empirically derived bias correction improves the agreement between GOSAT XCO_2/XCH_4 and the aircraft data. Finally, we present spatial distributions and temporal variations of the derived GOSAT biases.

1 Introduction

Atmospheric carbon dioxide (CO_2) and methane (CH_4) are crucially important anthropogenic greenhouse gases that contribute to global warming and future climate change. The Greenhouse gases Observing SATellite (GOSAT), launched in January 2009, is the world's first satellite specialized for measuring the concentrations of atmospheric CO_2 and CH_4 from space (Yokota et al., 2009). Column-averaged dry air mole fractions of CO_2 (XCO_2) and CH_4 (XCH_4) are retrieved from the Short-Wavelength InfraRed (SWIR) spectra of the Thermal And Near-infrared Sensor for carbon Observation – Fourier Transform Spectrometer (TANSO-FTS) onboard GOSAT. Validation of XCO_2 and XCH_4 derived from the GOSAT TANSO-FTS has been conducted by using ground-based high-resolution Fourier Transform Spectrometer (ground-based FTS) data and aircraft measurements (Morino et al., 2011; Saitoh et al., 2012; Yoshida et al., 2013; Inoue et al., 2013, 2014; Gavrilov et al., 2014). The results showed that the GOSAT SWIR XCO_2 measurements (Ver. 02.00) are biased -1–2 ppm ($\pm$1–3 ppm) against the aircraft measurement data (Inoue et al., 2013), whereas GOSAT SWIR XCH_4 measurements (Ver. 02.00) are biased positively by 2–7 ppb with a standard deviation of about 15 ppb (Inoue et al., 2014).

The systematic biases of the GOSAT XCO_2 and XCH_4 retrievals are produced by many factors including aerosol optical depth, thin cirrus clouds, and surface pressure retrieval error (e.g., Uchino et al., 2012; Yoshida et al., 2013). These biases can lead to large errors in the estimations of regional fluxes of CO_2 and CH_4 from inversion analyses (Takagi et al., 2011; Maksyutov et al., 2013; Deng et al., 2014; Ishizawa et al., 2016b). Consequently, several studies have described bias corrections of the satellite retrieval data by using linear regression (e.g., Wunch et al., 2011b; Cogan et al., 2012; Guerlet et al., 2013; Schneising et al., 2013; Nguyen et al., 2014). Wunch et al. (2011b) have attempted to correct spatially and temporally varying biases in the Atmospheric CO_2 Observations from Space retrievals of the GOSAT (ACOS-GOSAT; O'Dell et al., 2012; Crisp et al., 2012) data obtained over land using an empirical linear regression model with which they correlated variabilities in XCO_2 retrievals with surface albedo, the difference between the retrieved and a priori surface pressure, airmass, and the oxygen A-band spectral radiance. They used the GOSAT data in the Southern Hemisphere as the reference values for the linear regression and evaluated the bias correction against the Total Carbon Column Observing Network (TCCON) data from the Northern Hemisphere. Following Wunch et al. (2011b), Cogan et al. (2012) performed bias correction of GOSAT XCO_2 data retrieved from the University of Leicester full physics (UoL-FP) retrieval algorithm using pseudo observations based on GEOS-Chem model calculations. Guerlet et al. (2013) used XCO_2 measurements from 12 TCCON sites around the world as a reference for correction of GOSAT XCO_2 data retrieved from the Netherlands Institute for Space Research/Karlsruhe Institute of Technology (SRON/KIT) full physics retrieval algorithm.

In this study, we develop a method for correcting the systematic biases of the GOSAT XCO_2 and XCH_4 retrievals (Ver. 02.21) provided by the National Institute for Environmental Studies (NIES-GOSAT; Yoshida et al., 2013). Similar to Guerlet et al. (2013), we explicitly use TCCON data from 22 sites throughout the world as reference values for the regression analysis. The regression variables and coefficients for correction of GOSAT data are determined separately for observations made over land and those made over the ocean, and we perform this analysis for both XCO_2 and XCH_4. Such a partitioning is sensible because in the SWIR XCO_2 and XCH_4 retrievals, the handling of the surface reflectance is different over land and ocean. In addition, the atmosphere over ocean is generally cleaner than that over land because of the absence of polluted air and aerosols from urban areas. These differences suggest that the bias characteristics of XCO_2 and XCH_4 retrieved over ocean differ from those over land.

This paper is structured as follows. Section 2 presents a brief note on the data sets used and analysis procedure. In Sect. 3, we show a detailed method for correcting GOSAT data and the results of the empirical correction. Our findings and conclusions are given in Sect. 4.

2 Data and analysis methods

2.1 XCO_2 and XCH_4 retrieved from GOSAT TANSO-FTS SWIR spectra

To monitor the spatial distribution of atmospheric greenhouse gases from space, GOSAT was launched on 23 January 2009 into a sun-synchronous orbit with an overpass time of roughly 13:00 local time (Kuze et al., 2009). Over a 3-day period, TANSO-FTS onboard GOSAT makes observations above several tens of thousands of ground points spread over the earth's surface. Measurements in the SWIR and thermal infrared (TIR) bands of TANSO-FTS allow the retrievals over cloud-free regions of XCO_2 and XCH_4, and CO_2 and CH_4 profiles, respectively. (Yoshida et al., 2011, 2013; Saitoh et al., 2012). More recently, Kuze et al. (2016) reported update on the performance of GOSAT TANSO-FTS sensor and important changes to the data product which has been made available to users. In this study, we used Ver. 02.21 XCO_2 and XCH_4 data (Yoshida et al., 2013), which cover the period from April 2009 to May 2014.

2.2 TCCON data

The Total Carbon Column Observing Network (TCCON) is a worldwide network of ground-based FTSs that provide time series of column-averaged abundances of various atmospheric constituents. These constituents, which include CO_2 and CH_4, are retrieved from near-infrared solar absorption spectra using a nonlinear least-squares fitting algorithm referred to as GFIT (Wunch et al., 2010, 2011a). The TCCON data have been used to compare with satellite data and model simulations (Dils et al., 2006; Morino et al., 2011; Schneising et al., 2012; Saito et al., 2012; Heymann et al., 2012; Oshchepkov et al., 2013; Yoshida et al., 2013; Belikov et al., 2013; Dils et al., 2014; Nguyen et al., 2014; Scheepmaker et al., 2015) and elucidate the temporal behavior of greenhouse gases (Wunch et al., 2009; Deutscher et al., 2010, 2014; Messerschmidt et al., 2010; Ishizawa et al., 2016a). In this study, we used TCCON data analyzed with the GGG2014 version of the standard TCCON retrieval algorithm (Wunch et al., 2015) for correction of GOSAT data. The TCCON data are available from the Carbon Dioxide Information Analysis Center (CDIAC) at http://tccon.ornl.gov. The distribution and basic information of 23 TCCON sites used for correction or validation analyses of GOSAT data are shown in Fig. 1a and Table 1, respectively. See Table 1 for the data reference in respective TCCON sites. The TCCON sites are distributed throughout the world including North America, Europe, Asia, and Oceania (Fig. 1a). Due to the absence of coincidence with GOSAT data at Ny-Ålesund, these TCCON XCO_2 and XCH_4 data were not used for correction of GOSAT data; they were, however, used for the analysis of latitudinal distributions described in Sect. 3.3.

2.3 Aircraft-based data

In order to test for remaining biases in the GOSAT data after applying the empirical correction developed using TCCON data, we use aircraft profile data provided by the Comprehensive Observation Network for TRace gases by AIrLiner (CONTRAIL) project (Machida et al., 2008), the NOAA Earth System Research Laboratory/Global Monitoring Division (ESRL/GMD; Xiong et al., 2008; Sweeney et al., 2015), the US Department of Energy (DOE; Biraud et al., 2013; Schmid et al., 2014), the National Institute for Environmental Studies (NIES; Machida et al., 2001), the Japan Meteorological Agency (JMA; Tsuboi et al., 2013), the HIAPER Pole-to-Pole Observations (HIPPO) project (Wofsy et al., 2011, 2012; Kort et al., 2012; Santoni et al., 2014), and an aircraft measurement campaign by NIES and the Japan Aerospace Exploration Agency (JAXA) (Tanaka et al., 2012). To calculate aircraft-based XCO_2 and XCH_4 (as described in the next paragraph), we also used tower data from the Meteorological Research Institute (MRI) in Tsukuba (Inoue and Matsueda, 1996, 2001) and the NOAA ESRL/GMD tall tower network in Park Falls, WI and West Branch, IA (Andrews et al., 2014). Details of the aircraft and tower measurements are described in Inoue et al. (2013) and Inoue et al. (2014), except for the JMA aircraft and ground-based measurements. The JMA aircraft measurements are conducted by utilizing the cargo aircraft C-130H of the Japan Ministry of Defense (MOD) to collect flask air samples once a month during a regular flight between the mainland of Japan and Minamitorishima, an island located nearly 2000 km southeast of Tokyo (Tsuboi et al., 2013). In addition, the JMA routinely obtains ground-based measurements at a height of 20 m over Minamitorishima. We used CO_2 and CH_4 profiles from around Minamitorishima derived from aircraft and ground-based data available via the World Data Centre for Greenhouse Gases (WDCGG) website (http://ds.data.jma.go.jp/gmd/wdcgg/). The typical JMA aircraft sampling altitudes were 0.5–6.5 km. Figure 1b and Table 2 show a global map and basic information, respectively, on every aircraft measurement site used in this study.

Aircraft-based XCO_2 and XCH_4 are calculated by applying the GOSAT SWIR column averaging kernels (CAK) by using the methods developed by Miyamoto et al. (2013) and Inoue et al. (2014), respectively. There is one difference in the aircraft XCH_4 calculation: Inoue et al. (2014) used fixed monthly climatologies for the CH_4 profiles above the tropopause and did not include the yearly trend in CH_4 concentration because of their short analysis period (June 2009 to July 2010). In this study, the yearly trend is explicitly taken into account. According to recent reports from the World Meteorological Organization (WMO), global CH_4 abundance increased from 1789 ppb in 2007 to a high of 1824 ppb in 2013 (WMO, 2008, 2014) with a growth rate of about 6 ppb yr^{-1}. Here, we included this mean annual trend

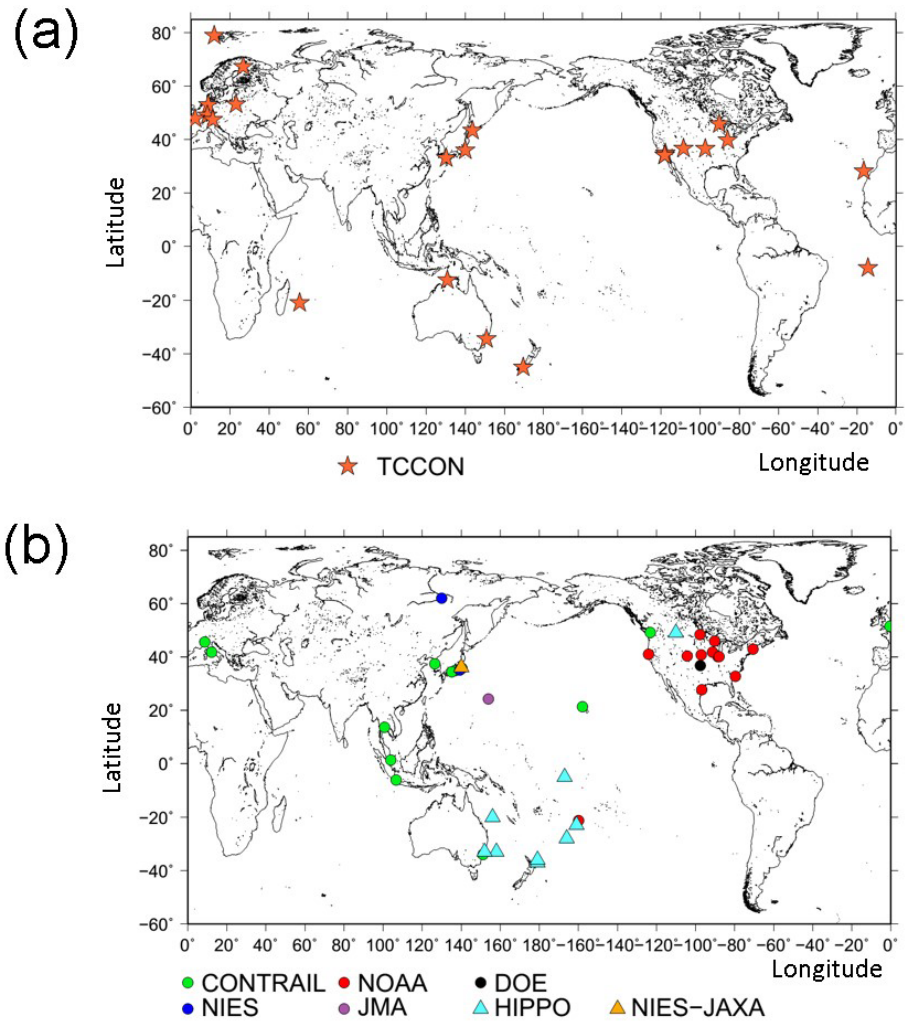

Figure 1. Global distributions of **(a)** the TCCON sites used for correction and validation of GOSAT data and **(b)** the aircraft observation sites used for validation of GOSAT data.

(6 ppb yr^{-1}) of CH_4 profiles above the tropopause for the calculation of aircraft-based XCH_4.

2.4 Correction and validation procedure of GOSAT data

Our aim in this study is to correct GOSAT SWIR XCO_2 and XCH_4 (Ver. 02.21) by multiple linear regression using TCCON data as reference values. In Sect. 3.1, we explain the details of the empirical correction method. To evaluate the effectiveness of this correction method, we compare uncorrected/corrected GOSAT XCO_2 (XCH_4) to independent aircraft-based XCO_2 (XCH_4) based on aircraft measurements by CONTRAIL, NOAA, DOE, NIES, JMA, the HIPPO project, and the NIES-JAXA joint campaign (Sect. 3.2). We compare GOSAT data retrieved on the same day and within ±5° latitude/longitude boxes centered on each aircraft profile. We also investigate the spatial distributions of uncorrected/corrected GOSAT data (Sect. 3.3), and the temporal behavior of the GOSAT XCO_2 and XCH_4 biases (Sect. 3.4).

3 Results and discussion

3.1 Parameter dependency of GOSAT biases and multiple linear regression for correction of GOSAT data

The bias correction of GOSAT XCO_2 and XCH_4 (Ver. 02.21) uses multiple linear regression. Before formulating the regression equations, we perform a correlation analysis between the GOSAT biases and simultaneously retrieved auxiliary parameters at TCCON sites. Here, the differences between GOSAT XCO_2 (XCH_4) and TCCON XCO_2 (XCH_4) are referred to as ΔXCO_2 (ΔXCH_4). Figures 2a–d and 3a show several examples of scatter diagrams between ΔXCO_2

Table 1. Basic information on the TCCON sites used for correction and validation of the GOSAT data.

Site	Latitude (deg. N)	Longitude (deg. E)	Elevation (m)	Region	Data reference (DOI number)
Ny-Ålesund	78.90	11.90	20	Spitzbergen, Norway	doi:10.14291/tccon.ggg2014.nyalesund01.R0/1149278
Sodankylä	67.37	26.63	188	Finland	doi:10.14291/tccon.ggg2014.sodankyla01.R0/1149280
Białystok	53.23	23.03	180	Poland	doi:10.14291/tccon.ggg2014.bialystok01.R1/1183984
Bremen	53.10	8.85	27	Germany	doi:10.14291/tccon.ggg2014.bremen01.R0/1149275
Karlsruhe	49.10	8.44	120	Germany	doi:10.14291/tccon.ggg2014.karlsruhe01.R1/1182416
Orléans	47.97	2.11	130	France	doi:10.14291/tccon.ggg2014.orleans01.R0/1149276
Garmisch	47.48	11.06	740	Germany	doi:10.14291/tccon.ggg2014.garmisch01.R0/1149299
Park Falls	45.95	−90.27	472	USA	doi:10.14291/tccon.ggg2014.parkfalls01.R0/1149161
Rikubetsu	43.46	143.77	361	Japan	doi:10.14291/tccon.ggg2014.rikubetsu01.R0/1149282
Indianapolis	39.86	−86.00	270	USA	doi:10.14291/tccon.ggg2014.indianapolis01.R0/1149164
Four Corners	36.80	−108.48	1643	USA	doi:10.14291/tccon.ggg2014.fourcorners01.R0/1149272
Lamont	36.60	−97.49	320	USA	doi:10.14291/tccon.ggg2014.lamont01.R0/1149159
Tsukuba	36.05	140.12	30	Japan	(120HR) doi:10.14291/tccon.ggg2014.tsukuba01.R0/1149281 (125HR) doi:10.14291/tccon.ggg2014.tsukuba02.R0/1149301
Edwards	34.96	−117.88	700	USA	doi:10.14291/tccon.ggg2014.edwards01.R0/1149289
JPL	34.20	−118.18	390	USA	doi:10.14291/tccon.ggg2014.jpl02.R0/1149297
Pasadena	34.14	−118.13	237	USA	doi:10.14291/tccon.ggg2014.pasadena01.R1/1182415
Saga	33.24	130.29	7	Japan	doi:10.14291/tccon.ggg2014.saga01.R0/1149283
Izaña	28.30	−16.50	2370	Tenerife, Canary Islands	doi:10.14291/tccon.ggg2014.izana01.R0/1149295
Ascension Island	−7.92	−14.33	31	South Atlantic Ocean	doi:10.14291/tccon.ggg2014.ascension01.R0/1149285
Darwin	−12.42	130.89	30	Australia	doi:10.14291/tccon.ggg2014.darwin01.R0/1149290
Reunion Island	−20.90	55.49	87	Indian Ocean	doi:10.14291/tccon.ggg2014.reunion01.R0/1149288
Wollongong	−34.41	150.88	30	Australia	doi:10.14291/tccon.ggg2014.wollongong01.R0/1149291
Lauder	−45.04	169.68	370	New Zealand	(120HR) doi:10.14291/tccon.ggg2014.lauder01.R0/1149293 (125HR) doi:10.14291/tccon.ggg2014.lauder02.R0/1149298

(or ΔXCH_4) and simultaneously retrieved auxiliary parameters obtained within ±5° latitude/longitude boxes centered at respective TCCON sites. The GOSAT data retrieved over land and ocean regions are described by green and blue dots, respectively. For instance, ΔXCO_2 has a significant negative correlation with the difference between the retrieved surface pressure and a priori surface pressure (ΔP_S; Fig. 2b), which suggests that error in the surface pressure retrieval (ΔP_S) is, in part, responsible for the presence of the GOSAT XCO_2 biases. Thus, we examined the correlations between the GOSAT biases and more than 20 other parameters retrieved from GOSAT TANSO-FTS, and investigated which combinations of available parameters led to a reduction of the GOSAT biases due to the linear regression. For the correction of XCO_2 retrievals, we selected four parameters to include in bias corrections; the retrieved aerosol optical depth (AOD), ΔP_S, airmass, and surface albedo for the O_2 A-band. The derived bias correction for XCO_2 is

$$\begin{aligned} X_{CO_2}^{\text{modified}} &= X_{CO_2}^{\text{retrieved}} + C_0 \\ &- C_1(\text{AOD} - \overline{\text{AOD}}) - C_2(\Delta P_S - \overline{\Delta P_S}) \\ &- C_3(\text{airmass} - \overline{\text{airmass}}) - C_4(\text{albedo\_O}_2 - \overline{\text{albedo\_O}_2}). \end{aligned} \quad (1)$$

However, only the retrieved AOD was selected for XCH_4 retrievals. The bias correction for XCH_4 is

$$X_{CH_4}^{\text{modified}} = X_{CH_4}^{\text{retrieved}} + C_0 - C_1(\text{AOD} - \overline{\text{AOD}}). \quad (2)$$

Here, $X_{CO_2}^{\text{retrieved}}$ and $X_{CH_4}^{\text{retrieved}}$ are the GOSAT XCO_2 and XCH_4 retrievals, respectively (i.e., uncorrected GOSAT data). $X_{CO_2}^{\text{modified}}$ and $X_{CH_4}^{\text{modified}}$ denote the corrected GOSAT XCO_2 and XCH_4 data, respectively. AOD represents the retrieved aerosol optical depth, and ΔP_S is the difference between the retrieved surface pressure and the a priori surface pressure. Airmass is a simple function of the solar zenith angle θ_Z and the satellite-viewing angle θ_V and can be approximated as

$$\text{airmass} = \frac{1}{\cos\theta_Z} + \frac{1}{\cos\theta_V}. \quad (3)$$

In addition, albedo_O_2 is the surface albedo for the O_2 A-band, which is retrieved only for land. The overbars denote averages of all GOSAT data used for the regression analysis. C_0 is the regression coefficient for the bias, and C_1, C_2, C_3, and C_4 are the regression coefficients for the respective parameters, that are used for the correction of GOSAT data. As described in the next paragraph, we determined these regression coefficients separately for land and ocean regions.

Table 2. Basic information on the aircraft observation sites used for validation of the GOSAT data.

Site code	Latitude (deg. N)	Longitude (deg. E)	Elevation (m)	Region	Site name
(a) CONTRAIL					
LHR	51.5	−0.5	24	London	Heathrow Airport
YVR	49.2	−123.2	4	Vancouver	Vancouver International Airport
MXP	45.6	8.7	24	Milan	Milan–Malpensa International Airport
FCO	41.8	12.3	5	Rome	Fiumicino Airport
ICN	37.5	126.5	7	Incheon	Incheon International Airport
NRT	35.8	140.4	43	Narita	Narita International Airport
HND	35.6	139.8	6	Haneda	Tokyo International Airport
NGO	34.9	136.8	5	Nagoya	Chubu Centrair International Airport
KIX	34.4	135.2	0	Kansai	Kansai International Airport
HNL	21.3	−157.9	4	Honolulu	Honolulu International Airport
BKK	13.7	100.7	2	Bangkok	Suvarnabhumi International Airport
SIN	1.4	104.0	7	Singapore	Singapore Changi International Airport
CGK	−6.1	106.7	10	Jakarta	Jakarta International Soekarno–Hatta Airport
SYD	−33.9	151.2	6	Sydney	Kingsford Smith Airport
(b) NOAA					
DND	48.4	−97.8	464	USA	Dahlen, North Dakota
LEF	45.9	−90.3	472	USA	Park Falls, Wisconsin
NHA	43.0	−70.6	0	USA	Worcester, Massachusetts
WBI	41.7	−91.4	242	USA	West Branch, Iowa
THD	41.1	−124.2	107	USA	Trinidad Head, California
BNE	40.8	−97.2	466	USA	Beaver Crossing, Nebraska
CAR	40.4	−104.3	1740	USA	Briggsdale, Colorado
HIL	40.1	−87.9	202	USA	Homer, Illinois
AAO	40.1	−88.6	213	USA	Airborne Aerosol Observing, Illinois
SCA	32.8	−79.6	0	USA	Charleston, South Carolina
TGC	27.7	−96.9	0	USA	Sinton, Texas
RTA	−21.3	−159.8	3	Cook Islands	Rarotonga
(c) DOE					
SGP	36.8	−97.5	314	USA	Southern Great Plains, Oklahoma
(d) NIES					
YAK	62	130	136	Russia	Yakutsk
SGM	35.1	139.3	0	Japan	Sagami Bay
(e) JMA					
MNM	24.3	154.0	8	Japan	Minamitorishima
(f) HIPPO					
HPA	49	−110	1040	USA	northeastern part of Great Falls, Montana
HPB	−28	−166	0	South Pacific Ocean	southwestern part of Rarotonga
HPC	−23	−161	0	South Pacific Ocean	southwestern part of Rarotonga
HPD	−33	158	0	Australia	eastern part of Lord Howe
HPE	−33	152	0	Australia	east coast of Newcastle
HPF	−20	156	0	Coral Sea	western part of Chesterfield Islands
HPG	−5	−167	0	Kiribati	western part of Enderbury
HPH	−37	179	0	New Zealand	northeastern part of Bay of Plenty
HPI	−36	179	0	New Zealand	northeastern part of Bay of Plenty
(g) NIES-JAXA					
TKB	36.1	140.1	31	Japan	Tsukuba

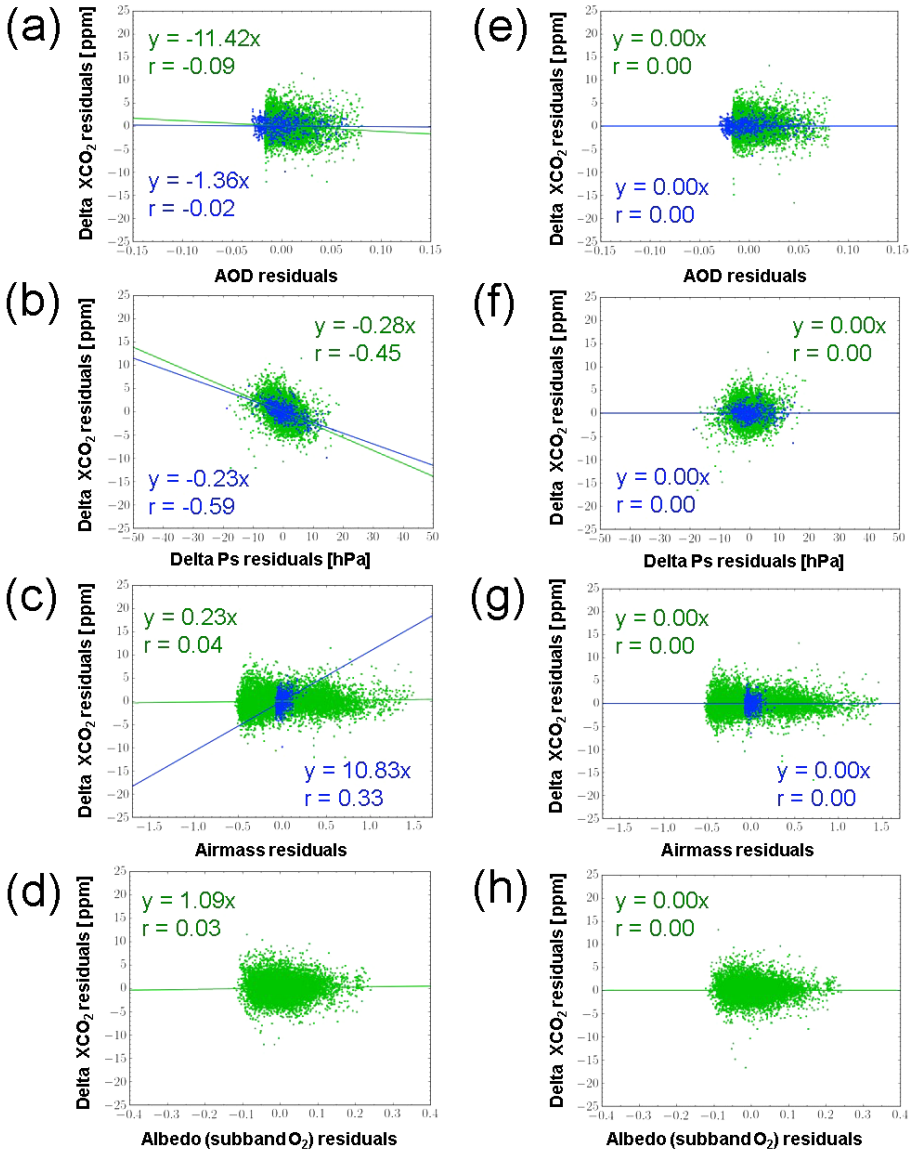

Figure 2. Scatter diagrams between ΔXCO_2 calculated from uncorrected GOSAT data and **(a)** the retrieved aerosol optical depth, **(b)** the difference between the retrieved and a priori surface pressures, **(c)** airmass, and **(d)** surface albedo for the O_2 A-band. Scatter diagrams between ΔXCO_2 calculated from corrected GOSAT data and **(e)** the retrieved aerosol optical depth, **(f)** the difference between the retrieved and a priori surface pressures, **(g)** airmass, and **(h)** surface albedo for the O_2 A-band. Green (blue) dots and lines indicate the GOSAT data and regression lines over land (ocean) regions.

Here, we discuss the spatiotemporal co-location criteria for calculations of the regression analyses. The ideal co-location criteria should be measurements at the same place during the same time (Zhou et al., 2016). In general, geographical co-location defines a spatiotemporal neighborhood region near the location of interest, and collects summary statistics (hereafter referred to as "geophysical co-location method", Cogan et al., 2012; Nguyen et al., 2014; Zhou et al., 2016). A disadvantage of the geophysical co-location method is that the number of matched data can become small when the spatiotemporal criteria are somewhat small. Therefore, several sophisticated methods were devised to obtain a sufficient number of co-located data. Following Keppel-Aleks et al. (2011) who implied a relationship between meridional gradients of free-tropospheric potential temperature and CO_2 concentrations in mid-latitudes over the Northern Hemisphere, Wunch et al. (2011b) used the distribution of potential temperature at 700 hPa when defining the co-location criteria in the Northern Hemisphere. Expansively, Nguyen et al. (2014) utilized a modified Euclidean distance weighted average of distance, time, and temperature at 700 hPa. Since this method is based on the fact that the

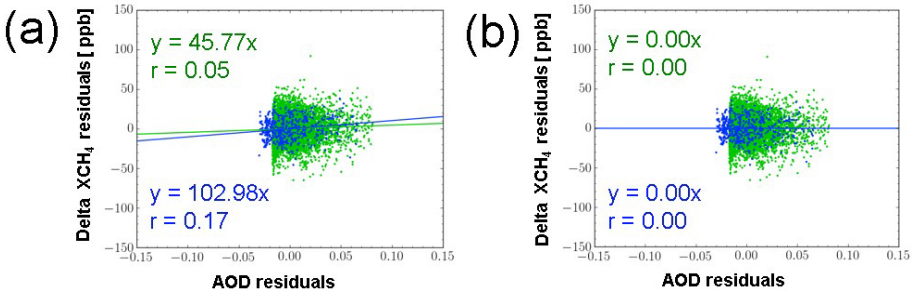

Figure 3. Scatter diagrams between ΔXCH_4 calculated from **(a)** uncorrected and **(b)** corrected GOSAT data and the retrieved aerosol optical depth. Green (blue) dots and lines indicate the GOSAT data and the regression lines over land (ocean) regions.

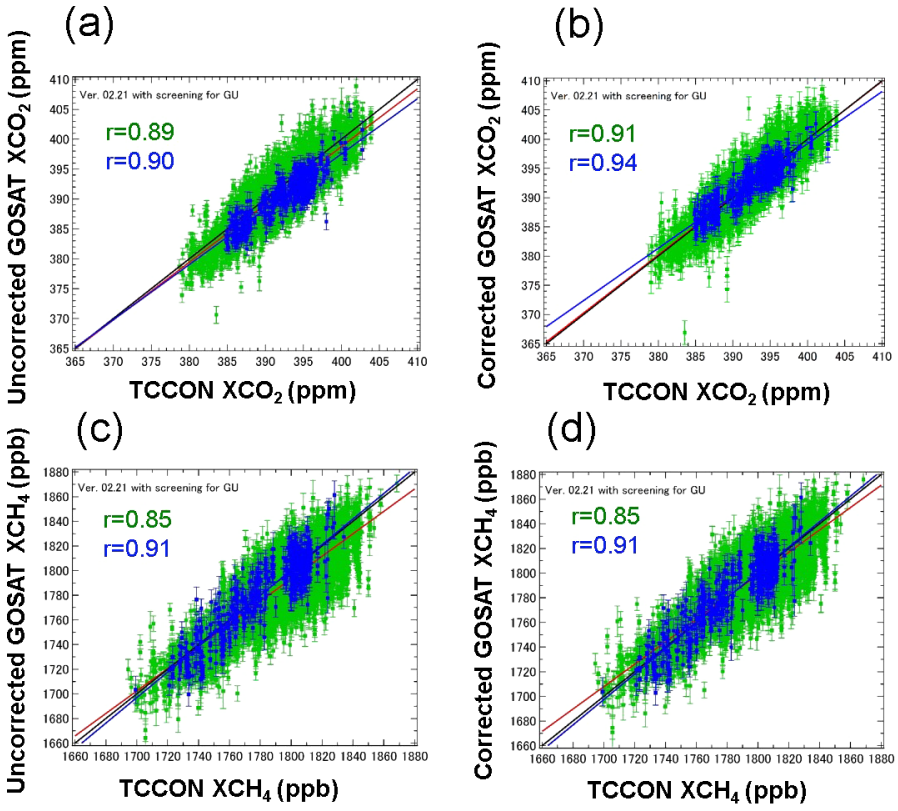

Figure 4. Scatter diagrams between **(a)** uncorrected and **(b)** corrected GOSAT XCO_2 observed within $\pm 5°$ latitude/longitude boxes (centered at each TCCON site) and TCCON XCO_2 measured on the same day. **(c, d)**, same as **(a)** and **(b)** for XCH_4. Green and blue dots indicate GOSAT data obtained over land and ocean regions, respectively. Red and blue lines denote the regression lines, statistically significant at the 99 % level, over land and ocean regions, respectively. Black lines show the one-to-one correspondence.

distribution of potential temperature at 700 hPa is deeply related to that of CO_2 density in the Northern Hemisphere, it is hard to apply this method to defining the co-location criteria in the low latitudes over the Northern Hemisphere and in the Southern Hemisphere. In addition, this method is not applicable to XCH_4. Guerlet et al. (2013) and Lindqvist et al. (2015) were based on the distribution of XCO_2 simulated by atmospheric transport model (e.g., the region where there is a modeled XCO_2 value within ± 0.5 ppm of standard deviation for the modeled value at the observation site). This can lead to much larger matched data and be applied to the entire globe including the Southern Hemisphere. However, reliable XCH_4 modeled data are hard to obtain, and the sophisticated method for XCH_4 remains to be established. In this study, 5 years of GOSAT SWIR V02.21 XCO_2 and XCH_4 data are used for the validation and correction. Because the number of available TCCON site has rapidly increased after the GOSAT launch, we can obtain enough matched data by the geophysical co-location method. Therefore, in this study, the coefficients C_0–C_4 were determined as follows:

Table 3. Values and errors of the regression coefficients for **(a)** XCO_2 and **(b)** XCH_4 retrievals calculated by multiple linear regression. The units of C_0, C_1, C_2, C_3, and C_4 for XCO_2 are (ppm), (ppm/units of AOD), (ppm/hPa), (ppm/airmass), and (ppm/units of albedo), respectively. The units of C_0 and C_1 for XCH_4 are (ppb) and (ppb/units of AOD), respectively.

(a)				
XCO_2	Land		Ocean	
Coefficients	Values	Errors	Values	Errors
C_0	0.865	0.021	1.903	0.055
C_1	−7.793	1.357	15.493	2.725
C_2	−0.282	0.006	−0.237	0.013
C_3	0.023	0.064	8.602	1.060
C_4	−2.036	0.433	–	–
(b)				
XCH_4	Land		Ocean	
	Values	Errors	Values	Errors
C_0	6.0	0.2	0.2	0.6
C_1	45.8	10.0	103.0	26.4

To prepare the TCCON XCO_2 and XCH_4 as reference values for the multiple regression analysis, we made a connection between the GOSAT data retrieved within ±5° latitude/longitude boxes centered at respective TCCON sites and mean values of TCCON data (GGG2014 version) observed within ±30 min of the GOSAT overpass time. Table 3 shows the regression coefficients obtained via the multiple linear regression analyses. Averages and the standard deviations (SD) of the differences between uncorrected GOSAT data and TCCON data at each site are listed in Table 4 for XCO_2 and Table 5 for XCH_4. Figure 4a and c are scatter diagrams between uncorrected GOSAT data and TCCON data at all TCCON sites for XCO_2 and XCH_4, respectively. For XCO_2, we identify 8245 samples for land and 544 samples for ocean that satisfy the coincident criteria. We find that global mean biases of GOSAT XCO_2 retrievals (i.e., uncorrected GOSAT XCO_2) over land and ocean regions against the TCCON data were −0.86 ppm (SD = 2.18 ppm) and −1.90 ppm (SD = 1.72 ppm), respectively (Table 4). The average and standard deviation of the GOSAT biases derived from respective TCCON sites (hereafter referred to as station bias) over land are −0.43 ppm and 0.87 ppm, respectively. Correlation coefficients between two XCO_2 data sets were 0.89 over land and 0.90 over ocean (Fig. 4a). The mean biases of uncorrected GOSAT XCH_4 over land and ocean regions were −6.0 ppb (SD = 15.2 ppb) and −0.2 ppb (SD = 13.4 ppb), respectively (Table 5). Correlation coefficients between both XCH_4 data sets were 0.85 over land and 0.91 over ocean (Fig. 4c). The results over land are similar to those of Yoshida et al. (2013) who validated GOSAT XCO_2 and XCH_4 data (Ver. 02.xx), although the versions of the TCCON data used in their study (the previous GGG2012 version) and our present study differ. Conducting the regression analysis using Eqs. (1) and (2), the regression coefficients for correction of GOSAT XCO_2 (and XCH_4) were determined separately for land and ocean regions (Table 3). Because surface albedo is not retrieved over ocean, the terms including C_4 in Eq. (1) were neglected for determining the regression coefficients for XCO_2 over ocean. The GOSAT data were obtained through two different TANSO-FTS modes: medium gain (Gain-M) utilized over bright land surfaces including the Sahara Desert and high gain (Gain-H) used elsewhere (Yoshida et al., 2013). Note that the regression coefficients are calculated from GOSAT data retrieved within ±5° boxes centered at 20 TCCON sites, that are located in Gain-H regions even though we aim to correct GOSAT XCO_2 and XCH_4 data from around the world, including Gain-H and Gain-M regions. Additionally, we take the mean difference between TCCON XCH_4 and aircraft-based XCH_4 into account when calculating the coefficients C_0 over land and ocean for XCH_4. In a comparative analysis at four locations, Inoue et al. (2014) showed that aircraft-based XCH_4 was 8.6 ppb smaller than TCCON XCH_4 on average. Consequently, in this study, we used the values for C_0 shown in Table 3b (i.e., 6.0 ppb over land and 0.2 ppb over ocean) for the correction of GOSAT XCH_4 when comparing GOSAT XCH_4 with TCCON XCH_4. In contrast, the values for C_0 shown in Table 3b with 8.6 ppb subtracted (i.e., −2.6 ppb over land and −8.4 ppb over ocean) were used when comparing the GOSAT XCH_4 with the aircraft-based XCH_4. Figures 2e–h and 3b are scatter diagrams between the biases of GOSAT data (ΔXCO_2 and ΔXCH_4) corrected by these regression coefficients C_0–C_4 (Table 3) and simultaneously retrieved parameters. After correction, the correlation coefficients between ΔXCO_2 (or ΔXCH_4) and respective parameters were approximately zero.

We compare the GOSAT XCO_2 and XCH_4 corrected using the regression coefficients to the TCCON XCO_2 and XCH_4 (Tables 4–5, and Figs. 4b and d). Using this empirical correction, the global mean biases of GOSAT XCO_2 relative to the TCCON data became zero over both land (change from −0.86 to 0.00 ppm) and ocean (−1.90 to −0.01 ppm). Correlation coefficients between GOSAT XCO_2 and TCCON XCO_2 became somewhat higher over land (0.89 to 0.91). Table 5 shows that the mean biases of GOSAT XCH_4 also became zero over both land (−6.0 to 0.0 ppb) and ocean (−0.2 to −0.1 ppb). Clearly, as expected, the GOSAT XCO_2 and XCH_4 biases were reduced after correction. This, of course, is a natural consequence because the GOSAT data approached the TCCON values after applying the corrections. Therefore, in the next section, we validate the GOSAT XCO_2 and XCH_4 corrected by TCCON data using independent aircraft measurement data instead of TCCON data.

Table 4. The average and standard deviation of the differences between uncorrected/corrected GOSAT XCO_2 and TCCON XCO_2 at each TCCON site. The GOSAT data were retrieved over **(a)** land and **(b)** ocean regions within $\pm 5^\circ$ latitude/longitude boxes centered at each site. The averages and standard deviations of the differences of the matched data at all TCCON sites (single scan) and those of the station biases are also shown in the second row from the bottom and the bottom row of the table, respectively.

(a) Land		Differences between uncorrected GOSAT XCO_2 and TCCON XCO_2		Differences between corrected GOSAT XCO_2 and TCCON XCO_2	
Site	number	average (ppm)	SD (ppm)	average (ppm)	SD (ppm)
Sodankylä	152	−0.03	1.93	0.48	1.92
Białystok	305	−0.18	2.22	0.79	2.05
Bremen	62	−0.10	1.98	0.46	1.52
Karlsruhe	229	0.35	2.27	0.85	2.01
Orléans	402	−0.26	2.00	0.24	1.82
Garmisch	326	0.23	2.42	0.70	2.17
Park Falls	482	−0.50	2.15	0.37	1.90
Rikubetsu	7	−0.92	1.32	−0.46	0.84
Indianapolis	158	−0.03	1.69	0.37	1.37
Four Corners	142	−1.17	1.95	0.07	1.87
Lamont	2767	−1.72	1.79	−0.49	1.61
Tsukuba	419	1.55	2.37	1.67	2.24
Edwards	38	−1.35	1.46	−0.49	1.10
JPL	264	−2.32	2.32	−1.01	2.33
Pasadena	109	−0.41	2.12	0.22	2.45
Saga	128	0.37	2.37	0.66	2.31
Izaña	56	0.47	1.34	0.92	1.04
Darwin	926	−1.16	1.51	−0.25	1.34
Wollongong	1071	−0.68	2.25	−0.05	2.25
Lauder	202	−0.77	1.79	−0.23	1.83
Total (single scan)	8245	−0.86	2.18	0.00	1.94
Total (station bias)	20	−0.43	0.87	0.24	0.62
(b) Ocean		Differences between uncorrected GOSAT XCO_2 and TCCON XCO_2		Differences between corrected GOSAT XCO_2 and TCCON XCO_2	
Site	number	average (ppm)	SD (ppm)	average (ppm)	SD (ppm)
Garmisch	5	−0.55	0.49	−0.67	0.83
Tsukuba	2	−2.87	2.35	−4.01	0.65
JPL	8	−4.71	3.64	−1.36	2.47
Saga	14	−1.15	2.56	−0.34	1.56
Izaña	50	−1.50	1.36	0.23	1.17
Ascension Island	234	−1.93	1.62	−0.17	1.18
Darwin	85	−1.64	1.86	0.54	1.56
Reunion Island	43	−2.19	1.43	−0.08	0.95
Wollongong	97	−2.04	1.49	0.05	1.04
Lauder	6	−2.54	2.32	0.53	0.87
Total (single scan)	544	−1.90	1.72	−0.01	1.29
Total (station bias)	10	−2.11	1.13	−0.53	1.35

Table 5. The average and standard deviation of the differences between uncorrected/corrected GOSAT XCH_4 and TCCON XCH_4 at each TCCON site. The GOSAT data were retrieved over **(a)** land and **(b)** ocean regions within $\pm 5^\circ$ latitude/longitude boxes centered at each site. The averages and standard deviations of the differences of the matched data at all TCCON sites (single scan) and those of the station biases are also shown in the second row from the bottom and the bottom row of the table, respectively.

(a) Land		Differences between uncorrected GOSAT XCH_4 and TCCON XCH_4		Differences between corrected GOSAT XCH_4 and TCCON XCH_4	
Site	number	average (ppb)	SD (ppb)	average (ppb)	SD (ppb)
Sodankylä	152	−2.3	11.4	3.8	11.4
Białystok	305	0.5	12.9	6.2	12.9
Bremen	62	−1.6	12.7	4.2	12.7
Karlsruhe	229	−0.9	15.3	5.0	15.3
Orléans	402	−3.9	12.7	2.0	12.7
Garmisch	326	6.2	16.3	11.9	16.3
Park Falls	482	3.3	13.9	9.2	13.9
Rikubetsu	7	4.1	8.6	9.7	8.8
Indianapolis	158	−1.4	10.9	5.0	10.9
Four Corners	142	−8.9	14.2	−3.0	14.3
Lamont	2767	−9.0	15.1	−2.9	15.2
Tsukuba	419	1.9	13.2	7.5	13.1
Edwards	38	−19.5	16.8	−13.2	16.7
JPL	264	−21.1	19.4	−15.1	19.4
Pasadena	109	−8.1	15.3	−1.8	15.3
Saga	128	−5.3	14.4	0.0	14.4
Izaña	56	15.4	12.7	20.1	13.1
Darwin	926	−8.6	8.9	−2.4	9.1
Wollongong	1076	−9.1	14.5	−2.8	14.7
Lauder	208	−3.9	11.3	2.4	11.2
Total (single scan)	8256	−6.0	15.2	0.0	15.2
Total (station bias)	20	−3.6	8.4	2.3	8.1
(b) Ocean		Differences between uncorrected GOSAT XCH_4 and TCCON XCH_4		Differences between corrected GOSAT XCH_4 and TCCON XCH_4	
Site	number	average (ppb)	SD (ppb)	average (ppb)	SD (ppb)
Garmisch	5	18.7	11.0	20.4	11.0
Tsukuba	2	21.9	16.0	21.2	17.2
JPL	8	−17.1	13.1	−17.4	12.9
Saga	14	0.7	17.0	−0.3	17.0
Izaña	50	14.8	7.7	14.1	8.4
Ascension Island	234	−1.0	11.5	−0.6	11.2
Darwin	85	4.1	13.2	3.0	13.3
Reunion Island	43	−0.4	8.3	0.1	8.9
Wollongong	97	−9.7	11.1	−8.6	11.7
Lauder	6	−5.9	11.9	−4.3	12.3
Total (single scan)	544	−0.2	13.4	−0.1	13.2
Total (station bias)	10	2.6	12.6	2.8	12.5

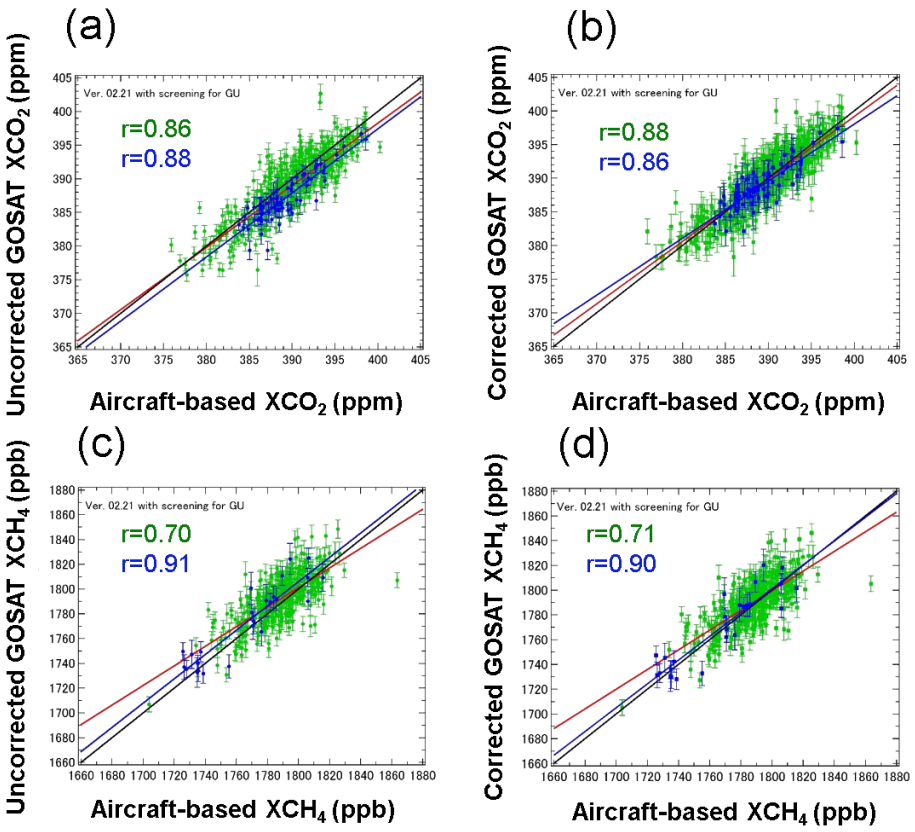

Figure 5. Scatter diagrams between **(a)** uncorrected and **(b)** corrected GOSAT XCO_2 observed within ±5° latitude/longitude boxes (centered on each aircraft profile) and aircraft-based XCO_2 observed on the same day. **(c, d)**, same as **(a)** and **(b)** for XCH_4. Green and blue dots indicate the GOSAT data obtained over land and ocean regions, respectively. Red and blue lines denote the regression lines, statistically significant at the 99 % level, over land and ocean regions, respectively. Black lines show the one-to-one correspondence.

3.2 Comparisons between uncorrected/corrected GOSAT data and aircraft-based data

To confirm the effectiveness of the empirical correction, we compare uncorrected/corrected GOSAT data with aircraft-based data. Figure 5 shows scatter diagrams between uncorrected/corrected GOSAT data and aircraft-based data at all aircraft observation sites. Tables 6 and 7 indicate the differences between uncorrected/corrected GOSAT data and aircraft-based data for XCO_2 and XCH_4 at each aircraft site, respectively. The average differences between uncorrected GOSAT XCO_2 and aircraft-based XCO_2 over land and ocean within ±5° latitude/longitude boxes were −0.85 ppm (SD = 2.48 ppm) and −2.08 ppm (SD = 1.69 ppm), respectively (Table 6). The correction reduced the mean biases of GOSAT XCO_2 to below twentieth over land (−0.85 to −0.04 ppm) and to below one-sixth over ocean (−2.08 to −0.32 ppm). The averages of the XCO_2 station bias over land and ocean are also smaller after correction. The correlation coefficients between GOSAT XCO_2 and aircraft-based XCO_2 over land became higher after correction (0.86 to 0.88). We here compare our results to those by other XCO_2 bias correction study. Cogan et al. (2012) showed the annual mean global difference to be reduced by about half (−1.22 to −0.68 ppm) and the correlation coefficients to increase from 0.61 to 0.74. Thus, our correction method is effective for removing the biases significantly. For XCH_4, the average differences between uncorrected GOSAT XCH_4 and aircraft-based XCH_4 over land and ocean were 4.5 ppb (SD = 15.2 ppb) and 6.6 ppb (SD = 12.8 ppb), respectively (Table 7). The global mean biases of corrected GOSAT XCH_4 relative to aircraft measurements were also reduced by half over land (4.5 to 2.2 ppb) and reduced to about one-quarter over ocean (6.6 to −1.7 ppb). The correlation coefficients between GOSAT XCH_4 and aircraft-based XCH_4 over land became higher (0.70 to 0.71). Thus, the bias correction improves the accuracy and precision of the GOSAT data for both XCO_2 and XCH_4.

3.3 Spatial distributions of uncorrected/corrected GOSAT data

We next applied the regression coefficients C_0–C_4 calculated from samples around only 22 TCCON sites to all GOSAT XCO_2 and XCH_4 data around the world, and we examined

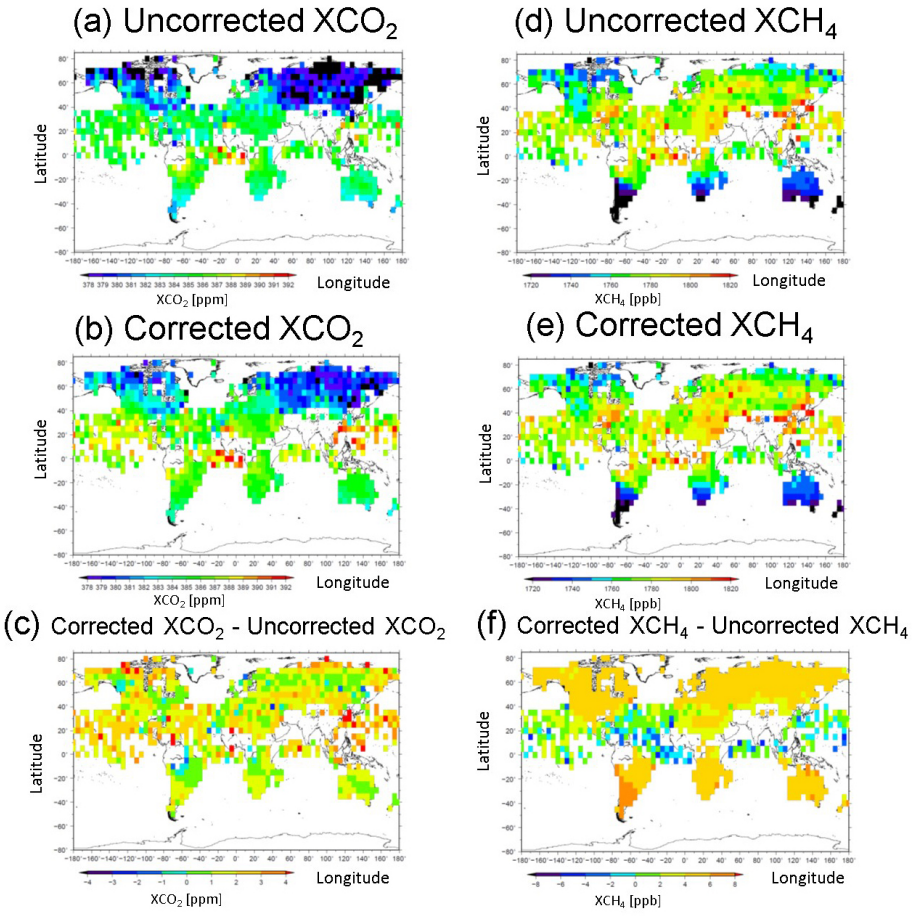

Figure 6. Global maps of the monthly means of **(a)** uncorrected and **(b)** corrected GOSAT XCO_2, and **(d)** uncorrected and **(e)** corrected GOSAT XCH_4 in July 2009. GOSAT XCO_2 and XCH_4 data were binned in 5° by 5° grid elements. The differences between corrected and uncorrected **(c)** GOSAT XCO_2 and **(f)** GOSAT XCH_4.

how the spatial distributions of GOSAT data changed due to this empirical correction. Figure 6a and b indicate the spatial distributions of the monthly means of uncorrected GOSAT XCO_2 and corrected GOSAT XCO_2, respectively, in July 2009. The GOSAT XCO_2 data were binned in 5° by 5° grid elements. In the northern summer, the CO_2 concentration over Siberia is significantly lower due to forest absorption of CO_2 through photosynthesis (e.g., Nakazawa et al., 1997; Guerlet et al., 2013). The differences between corrected GOSAT XCO_2 and uncorrected GOSAT XCO_2 are shown in Fig. 6c. As noted above, GOSAT XCO_2 has a negative bias of about 1–2 ppm over land and ocean regions. Therefore, the bias correction increases XCO_2 in most parts of the world (Fig. 6c). In the middle of South America and southern Africa, however, GOSAT XCO_2 became smaller after correction. The differences between corrected XCO_2 and uncorrected XCO_2 were about 2-4 ppm and less than 2 ppm in western part and eastern part of North America, respectively (Fig. 6c). This larger spatial gradient over North America is consistent with the result of Guerlet et al. (2013), though the months analyzed in their study (August and September) and our present study (July) differ. This feature over North America may be due to the differences in the type and condition of vegetation which have a strong impact on the surface albedo. Finally, this can have an influence on the estimation of regional CO_2 fluxes over North America by inverse analysis. We next focus on the spatial distributions of uncorrected/corrected GOSAT XCH_4 in July 2009 (Fig. 6d and e). Figure 6d shows that CH_4 concentrations in the Northern Hemisphere are higher than those in the Southern Hemisphere. In particular, there are distinct features of high CH_4 concentrations around the eastern United States, the Middle East, western Siberia, and East Asia in the Northern Hemisphere and low CH_4 concentrations over southern South America, southern Africa, and Australia, with a larger gradient in the Southern Hemisphere. After correction, GOSAT XCH_4 became 4–8 ppb higher over most land regions (Fig. 6f), consistent with comparisons to the TCCON data over land (Sect. 3.1). XCH_4 over the ocean became smaller at low latitudes in the Northern Hemisphere

Table 6. The average and standard deviation of the differences between uncorrected/corrected GOSAT XCO_2 and aircraft-based XCO_2 at each aircraft observation site. The GOSAT data were retrieved over **(a)** land and **(b)** ocean regions within $\pm 5^\circ$ latitude/longitude boxes centered at each site. The averages and standard deviations of the differences of the matched data at all aircraft observation sites (single scan) and those of the station biases are also shown in the second row from the bottom and the bottom row of the table, respectively.

(a) Land		Differences between uncorrected GOSAT XCO_2 and aircraft-based XCO_2		Differences between corrected GOSAT XCO_2 and aircraft-based XCO_2	
Site	number	average (ppm)	SD (ppm)	average (ppm)	SD (ppm)
LHR	3	−3.24	1.25	−2.09	0.66
YVR	7	−0.64	2.07	0.21	1.95
MXP	2	0.06	1.88	1.09	1.54
ICN	1	0.64	–	3.37	–
NRT	69	0.17	2.52	0.54	2.34
HND	2	−0.38	2.56	0.09	3.83
NGO	15	0.27	2.47	0.73	2.39
KIX	5	−1.01	3.25	−0.19	2.73
BKK	5	−2.90	3.86	−1.78	3.43
SYD	22	−1.19	2.48	−0.62	2.19
DND	11	−1.37	1.74	−0.47	1.48
LEF	34	0.02	2.77	0.66	2.79
NHA	25	0.27	1.64	0.44	1.69
WBI	23	−0.95	2.92	0.17	2.43
THD	4	−1.99	1.64	−0.06	1.13
BNE	6	−1.15	2.48	0.15	2.02
CAR	51	−2.17	2.20	−0.73	1.93
HIL	37	−2.16	1.96	−1.25	2.33
AAO	20	−0.18	2.32	0.64	2.28
SCA	22	−0.31	1.56	−0.01	1.60
TGC	15	−0.51	2.53	0.45	3.02
SGP	68	−1.61	2.20	−0.43	2.03
YAK	3	1.70	2.89	1.79	2.59
SGM	6	1.02	3.11	1.63	2.71
HPA	1	−2.84	–	−0.76	–
HPH	1	−1.91	–	−0.71	–
TKB	11	0.11	1.89	0.17	1.68
Total (single scan)	469	−0.85	2.48	−0.04	2.28
Total (station bias)	27	−0.82	1.24	0.11	1.11

(b) Ocean		Differences between uncorrected GOSAT XCO_2 and aircraft-based XCO_2		Differences between corrected GOSAT XCO_2 and aircraft-based XCO_2	
Site	number	average (ppm)	SD (ppm)	average (ppm)	SD (ppm)
FCO	1	0.12	–	−3.39	–
NRT	4	−4.27	3.24	−2.89	2.49
HND	1	0.86	–	2.51	–
NGO	3	−1.43	0.77	−0.02	0.58
KIX	4	−3.00	1.95	−1.86	1.56
HNL	19	−1.49	1.06	0.66	1.36
BKK	2	−3.40	0.96	−1.10	0.24
SIN	4	−2.33	1.70	0.06	2.05
CGK	2	−2.46	3.12	0.57	0.25
SYD	5	−1.52	1.28	−0.03	1.04
NHA	3	−1.56	1.07	−1.60	2.06
SCA	5	−2.67	2.05	−0.45	1.99
TGC	2	−2.36	0.12	−0.52	0.02
RTA	6	−2.93	1.75	−0.39	1.36
MNM	3	−1.39	0.61	−0.45	1.41
HPB	1	−0.16	–	0.86	–
HPD	1	-2.21	–	0.07	–
HPG	1	−3.29	–	−1.89	–
Total (single scan)	67	−2.08	1.69	−0.32	1.74
Total (station bias)	18	−1.97	1.31	−0.55	1.41

Table 7. The average and standard deviation of the differences between uncorrected/corrected GOSAT XCH_4 and aircraft-based XCH_4 at each aircraft observation site. The GOSAT data were retrieved over **(a)** land and **(b)** ocean regions within ±5° latitude/longitude boxes centered at each site. The averages and standard deviations of the differences of the matched data at all aircraft observation sites (single scan) and those of the station biases are also shown in the second row from the bottom and the bottom row of the table, respectively.

(a) Land		Differences between uncorrected GOSAT XCH_4 and aircraft-based XCH_4		Differences between corrected GOSAT XCH_4 and aircraft-based XCH_4	
Site	number	average (ppb)	SD (ppb)	average (ppb)	SD (ppb)
DND	12	7.3	10.0	5.0	10.0
LEF	33	9.3	19.9	7.1	19.8
NHA	26	7.4	14.6	5.2	14.4
WBI	19	5.3	12.7	2.7	13.2
THD	4	−15.6	20.3	−17.9	20.6
BNE	5	9.4	9.1	7.0	9.0
CAR	44	5.6	13.7	3.2	14.1
HIL	32	2.6	14.3	0.1	14.2
AAO	21	0.6	15.4	−2.1	15.3
SCA	20	7.9	12.4	5.9	12.4
TGC	13	8.7	16.2	6.7	16.4
SGP	69	0.4	15.7	−1.8	15.8
YAK	8	3.0	17.6	0.4	17.5
SGM	7	2.7	9.4	−0.3	9.3
HPA	1	−10.6	–	−12.5	–
HPI	1	3.0	–	1.5	–
TKB	11	10.8	12.4	8.5	12.0
Total (single scan)	326	4.5	15.2	2.2	15.3
Total (station bias)	17	3.4	7.0	1.1	7.0
(b) Ocean		Differences between uncorrected GOSAT XCH_4 and aircraft-based XCH_4		Differences between corrected GOSAT XCH_4 and aircraft-based XCH_4	
Site	number	average (ppb)	SD (ppb)	average (ppb)	SD (ppb)
NHA	3	24.2	10.9	16.7	10.1
SCA	5	−4.9	9.1	−13.6	9.6
TGC	2	9.5	2.3	3.1	2.8
RTA	7	5.2	14.5	−3.0	15.2
MNM	4	13.1	8.2	3.6	8.0
HPC	1	−2.2	–	−7.9	–
HPE	1	7.5	–	1.4	–
HPF	1	4.9	–	−3.5	–
HPG	1	−0.2	–	−13.8	–
Total (single scan)	25	6.6	12.8	−1.7	13.3
Total (station bias)	9	6.4	8.8	−1.9	9.6

(0°–20° N) such as the Atlantic Ocean, and became larger in mid-latitudes (20°–40° N).

It is difficult to evaluate whether the GOSAT data across the globe are improved by using the regression coefficients C_0–C_4 derived exclusively from around TCCON sites, due to the sparseness of the ground-based and aircraft measurements in many regions around the world. Accordingly, we investigated the latitudinal distributions of the uncorrected/corrected GOSAT data, the TCCON data, and the aircraft-based data, and then compared the three data sets for July 2009 (Fig. 7). We prepared zonal-mean monthly averages of the GOSAT data retrieved in each 15° latitu-

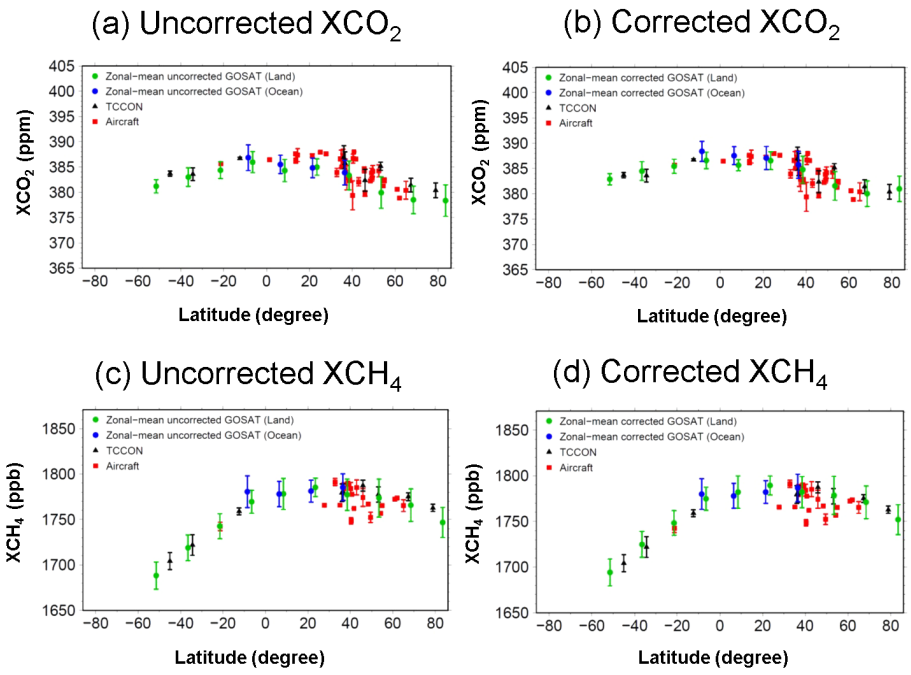

Figure 7. Latitudinal distributions of **(a)** uncorrected and **(b)** corrected GOSAT XCO_2, TCCON XCO_2, and aircraft-based XCO_2 in July 2009. Latitudinal distributions of **(c)** uncorrected and **(d)** corrected GOSAT XCH_4, TCCON XCH_4, and aircraft-based XCH_4 in July 2009. Green and blue circles indicate the zonal-mean GOSAT data retrieved over land and ocean regions, respectively. The black triangles and red squares denote the TCCON data and aircraft-based data, respectively, at each observation site. See text for details.

dinal band. For example, averages of GOSAT XCO_2 obtained over land and ocean regions within a latitudinal band from the equator to 15° N in July 2009 are represented by green and blue dots, respectively, around 7.5° N in Fig. 7a. The TCCON data are mean values measured within ±30 min of the GOSAT overpass time (e.g., about 12:50 pm local time in Tsukuba) on all days when TCCON data were obtained in July 2009. Aircraft-based data are monthly averages of all data obtained at each aircraft observation site. In July 2009, uncorrected GOSAT XCO_2 data were underestimated by about 1–2 ppm compared to the reference data (Fig. 7a). We found that corrected GOSAT XCO_2 was consistent with the TCCON XCO_2 and aircraft-based XCO_2 in both hemispheres, though the variability of aircraft-based XCO_2 was relatively large in mid-latitudes (Fig. 7b). Aircraft-based XCO_2 at the Honolulu site located around 20° N in July 2009 was 387.25 ppm. The uncorrected GOSAT XCO_2 and corrected GOSAT XCO_2 over the land regions around 20° N including Honolulu were 385.00 and 386.56 ppm, respectively, whereas those over the ocean regions were 384.82 and 387.07 ppm, respectively. By the correction, it was shown that GOSAT XCO_2 approached the aircraft-based XCO_2 value over both land and ocean. TCCON XCO_2 at Lauder was 383.71 ppm, and the uncorrected GOSAT XCO_2 and corrected GOSAT XCO_2 around 50° S including the Lauder site were 381.18 and 382.88 ppm, respectively. In the Southern Hemisphere, we found that GOSAT XCO_2 approached the TCCON value by the correction. Figure 7c shows latitudinal distributions of uncorrected GOSAT XCH_4, TCCON XCH_4, and aircraft-based XCH_4. XCH_4 in the Northern Hemisphere is higher than that in the Southern Hemisphere in July (Fig. 7c), because the main CH_4 sources are terrestrial, including rice paddy fields and wetlands. In addition, the latitudinal variation in XCH_4 shows a larger meridional gradient in the Southern Hemisphere (Fig. 7c), which is consistent with the spatial distribution of XCH_4 (Fig. 6d). The uncorrected GOSAT XCH_4 was negatively biased against the TCCON data. The empirical correction resulted in a marked decrease in GOSAT XCH_4 biases on the same latitudinal bands as several TCCON sites (e.g., Ny-Ålesund, Sodankylä, and Lauder) over both hemispheres (Fig. 7d). For example, TCCON XCH_4 at the Ny-Ålesund site was 1762.9 ppb, and the uncorrected GOSAT XCH_4 and corrected GOSAT XCH_4 around 80° N including Ny-Ålesund were 1746.8 and 1752.0 ppb, respectively. By the bias correction, GOSAT XCH_4 approached the TCCON value. Thus, the correction method is very effective for reducing the biases of the GOSAT XCO_2 and XCH_4, from the standpoint of the spatial distributions.

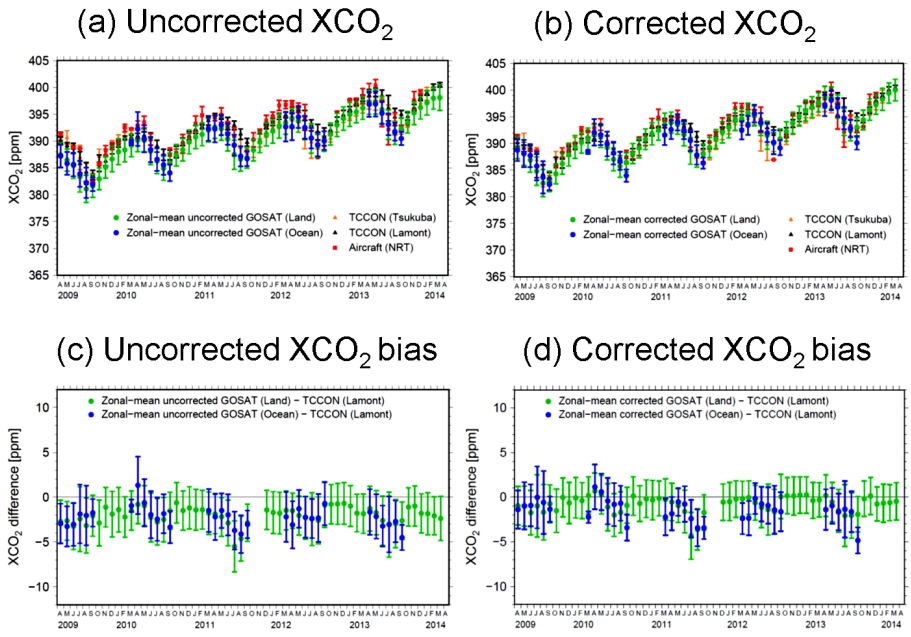

Figure 8. Temporal variations of **(a)** uncorrected and **(b)** corrected GOSAT XCO_2, TCCON XCO_2, and aircraft-based XCO_2. Green and blue circles in **(a)** and **(b)** indicate the monthly zonal-mean GOSAT data retrieved over land and ocean regions, respectively, within a 30°–45° N latitudinal band. The orange triangles, black triangles, and red squares in **(a)** and **(b)** denote the TCCON XCO_2 at Tsukuba and Lamont, and aircraft-based XCO_2 at Narita, respectively. Temporal variations of the differences between **(c)** uncorrected and **(d)** corrected GOSAT XCO_2 and TCCON XCO_2 at Lamont (GOSAT XCO_2 minus TCCON XCO_2) over land (green circles) and ocean (blue circles). See text for details.

3.4 Temporal behaviors of uncorrected/corrected GOSAT data and the GOSAT biases

Finally, we investigated temporal variations in GOSAT XCO_2 and XCH_4 data and the GOSAT biases. We focused on the 30°–45° N latitudinal band, which includes the Lamont site where most monthly data were available during the analysis period. Figure 8a shows the temporal variations of uncorrected GOSAT XCO_2, TCCON XCO_2 at Tsukuba and Lamont, and aircraft-based XCO_2 at Narita. Along with the example of July 2009 in Sect. 3.3, zonal-mean GOSAT XCO_2 retrieved over land and ocean regions within a 30°–45° N latitudinal band, TCCON XCO_2 and aircraft-based XCO_2 at several sites included in a 30°–45° N latitudinal band were calculated for all months during the analysis period. The temporal variations in the three data sets revealed that XCO_2 is higher in northern spring (April and May) and lower in August and September (Fig. 8a). XCO_2 has a seasonal amplitude of approximately 7–12 ppm at mid-latitudes over the Northern Hemisphere. In this study, the growth rate of uncorrected GOSAT XCO_2 was roughly 2.5 ppm yr^{-1} from 2009 to 2013, while Inoue et al. (2013) showed that the growth rate of aircraft-based XCO_2 at most sites was about 2.0 ppm yr^{-1} from 2007 to 2010. This is consistent with the rapid increase of CO_2 emissions over the last few years. After bias correction, the temporal variability in the GOSAT XCO_2 agrees with those of the TCCON and aircraft measurements (Fig. 8b). To clarify it, we show the monthly variations of the differences between uncorrected and corrected GOSAT XCO_2 and TCCON XCO_2 at Lamont (Fig. 8c and d). The uncorrected GOSAT XCO_2 data were negatively biased (Fig. 8c); however, this time series has a seasonality wherein the negative biases of GOSAT XCO_2 become higher around July and August. After bias correction, the XCO_2 biases for many months approach zero, though the seasonality in the difference remains (Fig. 8d). Note that the TCCON XCO_2 data at Lamont are values at a particular location, while GOSAT XCO_2 data are zonal averaged values.

Figure 9a shows the temporal behavior of zonal-mean uncorrected GOSAT XCH_4 and XCH_4 at the Tsukuba and Lamont TCCON sites. GOSAT XCH_4 is higher in September and October, and lower in February and March than the reference data. Although the GOSAT XCH_4 data retrieved over land were negatively biased except for summer during the analysis period (Fig. 9a and c), the GOSAT XCH_4 biases were reduced as a result of the empirical correction (Fig. 9b and d). Consequently, we suggest that the bias correction method was effective for GOSAT XCO_2 and XCH_4.

4 Summary and conclusions

In this study, we correct XCO_2 and XCH_4 data (Ver. 02.21) retrieved from the GOSAT TANSO-FTS SWIR spectra. First, we conducted correlation analyses between the GOSAT biases and the simultaneously retrieved auxiliary pa-

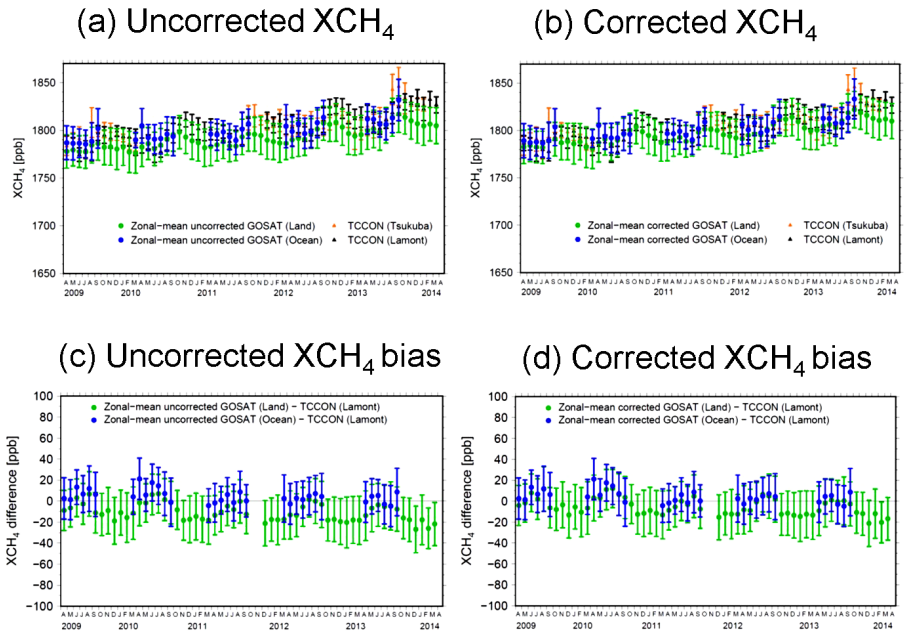

Figure 9. Temporal variations of **(a)** uncorrected and **(b)** corrected GOSAT XCH_4 and TCCON XCH_4. Green and blue circles in **(a)** and **(b)** indicate the monthly zonal-mean GOSAT data retrieved over land and ocean regions within a 30°–45° N latitudinal band, respectively. The orange and black triangles in **(a)** and **(b)** denote the TCCON XCH_4 at Tsukuba and Lamont, respectively. Temporal variations of the differences between **(c)** uncorrected and **(d)** corrected GOSAT XCH_4 and TCCON XCH_4 at Lamont (GOSAT XCH_4 minus TCCON XCH_4) over land (green circles) and ocean (blue circles). See text for details.

rameters, using GOSAT data around TCCON sites. Based on the results, we selected several parameters and determined the regression coefficients for the correction of GOSAT XCO_2 and XCH_4 for land and ocean regions separately. To evaluate the effectiveness of the bias correction method, the uncorrected/corrected GOSAT XCO_2 and XCH_4 data were compared to aircraft measurements provided by CONTRAIL, NOAA, DOE, NIES, JMA, the HIPPO project, and the NIES-JAXA joint campaign. After correction, biases of GOSAT XCO_2 were reduced by a factor of more than 20 over land and by a factor of 6 over ocean, while the biases of GOSAT XCH_4 were reduced by half over land and became by almost a quarter of their uncorrected values over ocean. We thus demonstrated that our empirical method using multiple linear regression is useful for the bias correction of GOSAT XCO_2 and XCH_4.

5 Data availability

The latest data processing and the auxiliary information on the GOSAT SWIR XCO_2 and XCH_4 data are described in GOSAT User Interface Gateway and can be obtained at http://data.gosat.nies.go.jp/GosatUserInterfaceGateway/guig/doc/documents/doc_en_docdist.html.

Acknowledgements. The authors thank the many staff members of Japan Airlines, the JAL Foundation, and JAMCO Tokyo for supporting the CONTRAIL project. We are grateful to the NOAA ESRL/GMD tall tower network (K. Davis, A. Desai, R. Teclaw, D. Baumann, and C. Stanier) for providing CO_2 tower data for Park Falls and West Branch. DOE flights were supported by the Office of Biological and Environmental Research of the US Department of Energy under contract no. DE-AC02-05CH11231 as part of the Atmospheric Radiation Measurement Program (ARM), ARM Aerial Facility, and Terrestrial Ecosystem Science Program. We gratefully thank many staff members of the Japan Ministry of Defense for supporting the JMA's ground-based and aircraft measurements. We also acknowledge the HIPPO team members for CO_2 and CH_4 profile data from HIPPO missions. The HIPPO program is supported by the National Science Foundation (NSF), and its operation is managed by the Earth Observing Laboratory (EOL) of the National Center for Atmospheric Research (NCAR). We also thank the Canadian Space Agency (CSA), which provides most of the funding support for ACE. We are grateful to the HALOE team for publishing their data for scientific use. This research was supported in part by the Environment Research and Technology Development Fund (2A-1102) of the Ministry of the Environment, Japan. TCCON measurements from Pasadena, Lamont, Park Falls and Darwin are funded by NASA grant NNX14AI60G and NASA Orbiting Carbon Observatory Program. We are grateful to the DOE ARM program for technical support of TCCON in Lamont and Darwin and to Jeff Ayers for technical support of the TCCON measurements in Park Falls. Darwin and Wollongong TCCON measurements are also supported by Australian Research

Council grant DP140101552 and Nicholas Deutscher is supported by an ARC-DECRA Fellowship, DE140100178. The University of Bremen acknowledges the support of the EU projects InGOS, and ICOS-INWIRE, and the Senate of Bremen for support of TCCON measurements in Białystok, Bremen, Ny-Ålesund, and Orléans. Operation of the Ascension Island site was funded by the Max Planck Society. Research at the FMI was supported by the Academy of Finland under grant no. 140408.

Edited by: I. Aben
Reviewed by: two anonymous referees

References

Andrews, A. E., Kofler, J. D., Trudeau, M. E., Williams, J. C., Neff, D. H., Masarie, K. A., Chao, D. Y., Kitzis, D. R., Novelli, P. C., Zhao, C. L., Dlugokencky, E. J., Lang, P. M., Crotwell, M. J., Fischer, M. L., Parker, M. J., Lee, J. T., Baumann, D. D., Desai, A. R., Stanier, C. O., De Wekker, S. F. J., Wolfe, D. E., Munger, J. W., and Tans, P. P.: CO_2, CO, and CH_4 measurements from tall towers in the NOAA Earth System Research Laboratory's Global Greenhouse Gas Reference Network: instrumentation, uncertainty analysis, and recommendations for future high-accuracy greenhouse gas monitoring efforts, Atmos. Meas. Tech., 7, 647–687, doi:10.5194/amt-7-647-2014, 2014.

Belikov, D. A., Maksyutov, S., Sherlock, V., Aoki, S., Deutscher, N. M., Dohe, S., Griffith, D., Kyro, E., Morino, I., Nakazawa, T., Notholt, J., Rettinger, M., Schneider, M., Sussmann, R., Toon, G. C., Wennberg, P. O., and Wunch, D.: Simulations of column-averaged CO_2 and CH_4 using the NIES TM with a hybrid sigma-isentropic (σ-θ) vertical coordinate, Atmos. Chem. Phys., 13, 1713–1732, doi:10.5194/acp-13-1713-2013, 2013.

Biraud, S. C., Torn, M. S., Smith, J. R., Sweeney, C., Riley, W. J., and Tans, P. P.: A multi-year record of airborne CO_2 observations in the US Southern Great Plains, Atmos. Meas. Tech., 6, 751–763, doi:10.5194/amt-6-751-2013, 2013.

Cogan, A. J., Boesch, H., Parker, R. J., Feng, L., Palmer, P. I., Blavier, J.-F. L., Deutscher, N. M., Macatangay, R., Notholt, J., Roehl, C., Warneke, T., and Wunch, D.: Atmospheric carbon dioxide retrieved from the Greenhouse gases Observing SATellite (GOSAT): Comparison with ground-based TCCON observations and GEOS-Chem model calculations, J. Geophys. Res., 117, D21301, doi:10.1029/2012JD018087, 2012.

Crisp, D., Fisher, B. M., O'Dell, C., Frankenberg, C., Basilio, R., Bösch, H., Brown, L. R., Castano, R., Connor, B., Deutscher, N. M., Eldering, A., Griffith, D., Gunson, M., Kuze, A., Mandrake, L., McDuffie, J., Messerschmidt, J., Miller, C. E., Morino, I., Natraj, V., Notholt, J., O'Brien, D. M., Oyafuso, F., Polonsky, I., Robinson, J., Salawitch, R., Sherlock, V., Smyth, M., Suto, H., Taylor, T. E., Thompson, D. R., Wennberg, P. O., Wunch, D., and Yung, Y. L.: The ACOS CO_2 retrieval algorithm – Part II: Global XCO_2 data characterization, Atmos. Meas. Tech., 5, 687–707, doi:10.5194/amt-5-687-2012, 2012.

Deng, F., Jones, D. B. A., Henze, D. K., Bousserez, N., Bowman, K. W., Fisher, J. B., Nassar, R., O'Dell, C., Wunch, D., Wennberg, P. O., Kort, E. A., Wofsy, S. C., Blumenstock, T., Deutscher, N. M., Griffith, D. W. T., Hase, F., Heikkinen, P., Sherlock, V., Strong, K., Sussmann, R., and Warneke, T.: Inferring regional sources and sinks of atmospheric CO_2 from GOSAT XCO_2 data, Atmos. Chem. Phys., 14, 3703–3727, doi:10.5194/acp-14-3703-2014, 2014.

Deutscher, N. M., Griffith, D. W. T., Bryant, G. W., Wennberg, P. O., Toon, G. C., Washenfelder, R. A., Keppel-Aleks, G., Wunch, D., Yavin, Y., Allen, N. T., Blavier, J.-F., Jiménez, R., Daube, B. C., Bright, A. V., Matross, D. M., Wofsy, S. C., and Park, S.: Total column CO_2 measurements at Darwin, Australia – site description and calibration against in situ aircraft profiles, Atmos. Meas. Tech., 3, 947–958, doi:10.5194/amt-3-947-2010, 2010.

Deutscher, N. M., Sherlock, V., Mikaloff Fletcher, S. E., Griffith, D. W. T., Notholt, J., Macatangay, R., Connor, B. J., Robinson, J., Shiona, H., Velazco, V. A., Wang, Y., Wennberg, P. O., and Wunch, D.: Drivers of column-average CO_2 variability at Southern Hemispheric Total Carbon Column Observing Network sites, Atmos. Chem. Phys., 14, 9883–9901, doi:10.5194/acp-14-9883-2014, 2014.

Dils, B., De Mazière, M., Müller, J. F., Blumenstock, T., Buchwitz, M., de Beek, R., Demoulin, P., Duchatelet, P., Fast, H., Frankenberg, C., Gloudemans, A., Griffith, D., Jones, N., Kerzenmacher, T., Kramer, I., Mahieu, E., Mellqvist, J., Mittermeier, R. L., Notholt, J., Rinsland, C. P., Schrijver, H., Smale, D., Strandberg, A., Straume, A. G., Stremme, W., Strong, K., Sussmann, R., Taylor, J., van den Broek, M., Velazco, V., Wagner, T., Warneke, T., Wiacek, A., and Wood, S.: Comparisons between SCIAMACHY and ground-based FTIR data for total columns of CO, CH_4, CO_2 and N_2O, Atmos. Chem. Phys., 6, 1953–1976, doi:10.5194/acp-6-1953-2006, 2006.

Dils, B., Buchwitz, M., Reuter, M., Schneising, O., Boesch, H., Parker, R., Guerlet, S., Aben, I., Blumenstock, T., Burrows, J. P., Butz, A., Deutscher, N. M., Frankenberg, C., Hase, F., Hasekamp, O. P., Heymann, J., De Mazière, M., Notholt, J., Sussmann, R., Warneke, T., Griffith, D., Sherlock, V., and Wunch, D.: The Greenhouse Gas Climate Change Initiative (GHG-CCI): comparative validation of GHG-CCI SCIAMACHY/ENVISAT and TANSO-FTS/GOSAT CO_2 and CH_4 retrieval algorithm products with measurements from the TCCON, Atmos. Meas. Tech., 7, 1723–1744, doi:10.5194/amt-7-1723-2014, 2014.

Gavrilov, N. M., Makarova, M. V., Poberovskii, A. V., and Timofeyev, Yu. M.: Comparisons of CH_4 ground-based FTIR measurements near Saint Petersburg with GOSAT observations, Atmos. Meas. Tech., 7, 1003–1010, doi:10.5194/amt-7-1003-2014, 2014.

GOSAT User Interface Gateway: GOSAT SWIR XCO_2 and XCH_4 data, available at: http://data.gosat.nies.go.jp/GosatUserInterfaceGateway/guig/doc/documents/doc_en_docdist.html, last access: 29 July 2016.

Guerlet, S., Basu, S., Butz, A., Krol, M., Hahne, P., Houweling, S., Hasekamp, O. P., and Aben, I.: Reduced carbon uptake during the 2010 Northern Hemisphere summer from GOSAT, Geophys. Res. Lett., 40, 2378–2383, doi:10.1002/grl.50402, 2013.

Heymann, J., Bovensmann, H., Buchwitz, M., Burrows, J. P., Deutscher, N. M., Notholt, J., Rettinger, M., Reuter, M., Schneising, O., Sussmann, R., and Warneke, T.: SCIAMACHY WFM-DOAS XCO_2: reduction of scattering related errors, Atmos. Meas. Tech., 5, 2375–2390, doi:10.5194/amt-5-2375-2012, 2012.

Inoue, H. Y. and Matsueda, H.: Variations in atmospheric CO_2 at the Meteorological Research Institute, Tsukuba, Japan, J. Atmos. Chem., 23, 137–161, 1996.

Inoue, H. Y. and Matsueda, H.: Measurements of atmospheric CO_2 from a meteorological tower in Tsukuba, Japan, Tellus B, 53, 205–219, doi:10.1034/j.1600-0889.2001.01163.x, 2001.

Inoue, M., Morino, I., Uchino, O., Miyamoto, Y., Yoshida, Y., Yokota, T., Machida, T., Sawa, Y., Matsueda, H., Sweeney, C., Tans, P. P., Andrews, A. E., Biraud, S. C., Tanaka, T., Kawakami, S., and Patra, P. K.: Validation of XCO_2 derived from SWIR spectra of GOSAT TANSO-FTS with aircraft measurement data, Atmos. Chem. Phys., 13, 9771–9788, doi:10.5194/acp-13-9771-2013, 2013.

Inoue, M., Morino, I., Uchino, O., Miyamoto, Y., Saeki, T., Yoshida, Y., Yokota, T., Sweeney, C., Tans, P. P., Biraud, S. C., Machida, T., Pittman, J. V., Kort, E. A., Tanaka, T., Kawakami, S., Sawa, Y., Tsuboi, K., and Matsueda, H.: Validation of XCH_4 derived from SWIR spectra of GOSAT TANSO-FTS with aircraft measurement data, Atmos. Meas. Tech., 7, 2987–3005, doi:10.5194/amt-7-2987-2014, 2014.

Ishizawa, M., Uchino, O., Morino, I., Inoue, M., Yoshida, Y., Mabuchi, K., Shirai, T., Tohjima, Y., Maksyutov, S., Ohyama, H., Kawakami, S., Takizawa, A., and Belikov, D.: Large XCH_4 anomaly in summer 2013 over northeast Asia observed by GOSAT, Atmos. Chem. Phys., 16, 9149–9161, doi:10.5194/acp-16-9149-2016, 2016a.

Ishizawa, M., Shirai, T., Inoue, M., Morino, I., Yoshida, Y., Zhuravlev, R., Ganshin, A., Belikov, D., Saito, M., Oda, T., Valsala, V., Uchino, O., Yokota, T., and Maksyutov, S.: Impact of retrieval biases of GOSAT XCO_2 on the surface CO_2 flux estimates, in preparation, 2016b.

Keppel-Aleks, G., Wennberg, P. O., and Schneider, T.: Sources of variations in total column carbon dioxide, Atmos. Chem. Phys., 11, 3581–3593, doi:10.5194/acp-11-3581-2011, 2011.

Kort, E. A., Wofsy, S. C., Daube, B. C., Diao, M., Elkins, J. W., Gao, R. S., Hintsa, E. J., Hurst, D. F., Jimenez, R., Moore, F. L., Spackman, J. R., and Zondlo, M. A.: Atmospheric observations of Arctic Ocean methane emissions up to 82° north, Nat. Geosci., 5, 318–321, doi:10.1038/ngeo1452, 2012.

Kuze, A., Suto, H., Nakajima, M., and Hamazaki, T.: Thermal and near infrared sensor for carbon observation Fourier-transform spectrometer on the Greenhouse Gases Observing Satellite for greenhouse gases monitoring, Appl. Optics, 48, 6716–6733 doi:10.1364/AO.48.006716, 2009.

Kuze, A., Suto, H., Shiomi, K., Kawakami, S., Tanaka, M., Ueda, Y., Deguchi, A., Yoshida, J., Yamamoto, Y., Kataoka, F., Taylor, T. E., and Buijs, H. L.: Update on GOSAT TANSO-FTS performance, operations, and data products after more than 6 years in space, Atmos. Meas. Tech., 9, 2445–2461, doi:10.5194/amt-9-2445-2016, 2016.

Lindqvist, H., O'Dell, C. W., Basu, S., Boesch, H., Chevallier, F., Deutscher, N., Feng, L., Fisher, B., Hase, F., Inoue, M., Kivi, R., Morino, I., Palmer, P. I., Parker, R., Schneider, M., Sussmann, R., and Yoshida, Y.: Does GOSAT capture the true seasonal cycle of carbon dioxide?, Atmos. Chem. Phys., 15, 13023–13040, doi:10.5194/acp-15-13023-2015, 2015.

Machida, T., Nakazawa, T., Ishidoya, S., Maksyutov, S., Tohjima, Y., Takahashi, Y., Watai, T., Vinnichenko, N., Panchenko, M., Arshinov, M., Fedoseev, N., and Inoue, G: Temporal and spatial variations of atmospheric CO_2 mixing ratio over Siberia, Ext. Abstr. 6th International CO_2 Conf., 1–5 October, Sendai, Japan, 2001.

Machida, T., Matsueda, H., Sawa, Y., Nakagawa, Y., Hirotani, K., Kondo, N., Goto, K., Nakazawa, T., Ishikawa, K., and Ogawa, T.: Worldwide measurements of atmospheric CO_2 and other trace gas species using commercial airlines, J. Atmos. Ocean. Tech., 25, 1744–1754, doi:10.1175/2008JTECHA1082.1, 2008.

Maksyutov, S., Takagi, H., Valsala, V. K., Saito, M., Oda, T., Saeki, T., Belikov, D. A., Saito, R., Ito, A., Yoshida, Y., Morino, I., Uchino, O., Andres, R. J., and Yokota, T.: Regional CO_2 flux estimates for 2009–2010 based on GOSAT and ground-based CO_2 observations, Atmos. Chem. Phys., 13, 9351–9373, doi:10.5194/acp-13-9351-2013, 2013.

Messerschmidt, J., Macatangay, R., Notholt, J., Petri, C., Warneke, T., and Weinzierl, C.: Side by side measurements of CO_2 by ground-based Fourier transform spectrometry (FTS), Tellus B, 62, 749–758, doi:10.1111/j.1600-0889.2010.00491.x, 2010.

Miyamoto, Y., Inoue, M., Morino, I., Uchino, O., Yokota, T., Machida, T., Sawa, Y., Matsueda, H., Sweeney, C., Tans, P. P., Andrews, A. E., Biraud, S. C., and Patra, P. K.: Atmospheric column-averaged mole fractions of carbon dioxide at 53 aircraft measurement sites, Atmos. Chem. Phys., 13, 5265–5275, doi:10.5194/acp-13-5265-2013, 2013.

Morino, I. Uchino, O., Inoue, M., Yoshida, Y., Yokota, T., Wennberg, P. O., Toon, G. C., Wunch, D., Roehl, C. M., Notholt, J., Warneke, T., Messerschmidt, J., Griffith D. W. T., Deutscher, N. M., Sherlock, V., Connor, B., Robinson, J., Sussmann, R., and Rettinger, M.: Preliminary validation of column-averaged volume mixing ratios of carbon dioxide and methane retrieved from GOSAT short-wavelength infrared spectra, Atmos. Meas. Tech., 4, 1061–1076, doi:10.5194/amt-4-1061-2011, 2011.

Nakazawa, T., Sugawara, S., Inoue, G., Machida, T., Maksyutov, S., and Mukai, H.: Aircraft measurements of the concentrations of CO_2, CH_4, N_2O, and CO and the carbon and oxygen isotopic ratios of CO_2 in the troposphere over Russia, J. Geophys. Res., 102, 3843–3859, 1997.

Nguyen, H., Osterman, G., Wunch, D., O'Dell, C., Mandrake, L., Wennberg, P., Fisher, B., and Castano, R.: A method for colocating satellite XCO_2 data to ground-based data and its application to ACOS-GOSAT and TCCON, Atmos. Meas. Tech., 7, 2631–2644, doi:10.5194/amt-7-2631-2014, 2014.

O'Dell, C. W., Connor, B., Bösch, H., O'Brien, D., Frankenberg, C., Castano, R., Christi, M., Eldering, D., Fisher, B., Gunson, M., McDuffie, J., Miller, C. E., Natraj, V., Oyafuso, F., Polonsky, I., Smyth, M., Taylor, T., Toon, G. C., Wennberg, P. O., and Wunch, D.: The ACOS CO_2 retrieval algorithm – Part 1: Description and validation against synthetic observations, Atmos. Meas. Tech., 5, 99–121, doi:10.5194/amt-5-99-2012, 2012.

Oshchepkov, S., Bril, A., Yokota, T., Wennberg, P. O., Deutscher, N. M., Wunch, D., Toon, G. C., Yoshida, Y., O'Dell, C. W., Crisp, D., Miller, C. E., Frankenberg, C., Butz, A., Aben, I., Guerlet, S., Hasekamp, O., Boesch, H., Cogan, A., Parker, R., Griffith, D., Macatangay, R., Notholt, J., Sussmann, R., Rettinger, M., Sherlock, V., Robinson, J., Kyrö, E., Heikkinen, P., Feist, D. G., Morino, I., Kadygrov, N., Belikov, D., Maksyutov, S., Matsunaga, T., Uchino, O., and Watanabe, H.: Effects of atmospheric light scattering on spectroscopic observations of greenhouse gases from space. Part 2: Algorithm intercomparison in the

GOSAT data processing for CO_2 retrievals over TCCON sites, J. Geophys. Res., 118, 1493–1512, doi:10.1002/jgrd.50146, 2013.

Saito, R., Patra, P. K., Deutscher, N., Wunch, D., Ishijima, K., Sherlock, V., Blumenstock, T., Dohe, S., Griffith, D., Hase, F., Heikkinen, P., Kyrö, E., Macatangay, R., Mendonca, J., Messerschmidt, J., Morino, I., Notholt, J., Rettinger, M., Strong, K., Sussmann, R., and Warneke, T.: Technical Note: Latitude-time variations of atmospheric column-average dry air mole fractions of CO_2, CH_4 and N_2O, Atmos. Chem. Phys., 12, 7767–7777, doi:10.5194/acp-12-7767-2012, 2012.

Saitoh, N., Touno, M., Hayashida, S., Imasu, R., Shiomi, K., Yokota, T., Yoshida, Y., Machida, T., Matsueda, H., and Sawa, Y.: Comparisons between XCH_4 from GOSAT Shortwave and Thermal Infrared Spectra and Aircraft CH_4 Measurement over Guam, Sci. Online Lett. Atmos. (SOLA), 8, 145–149, doi:10.2151/sola.2012-036, 2012.

Santoni, G. W., Daube, B. C., Kort, E. A., Jiménez, R., Park, S., Pittman, J. V., Gottlieb, E., Xiang, B., Zahniser, M. S., Nelson, D. D., McManus, J. B., Peischl, J., Ryerson, T. B., Holloway, J. S., Andrews, A. E., Sweeney, C., Hall, B., Hintsa, E. J., Moore, F. L., Elkins, J. W., Hurst, D. F., Stephens, B. B., Bent, J., and Wofsy, S. C.: Evaluation of the airborne quantum cascade laser spectrometer (QCLS) measurements of the carbon and greenhouse gas suite – CO_2, CH_4, N_2O, and CO – during the CalNex and HIPPO campaigns, Atmos. Meas. Tech., 7, 1509–1526, doi:10.5194/amt-7-1509-2014, 2014.

Scheepmaker, R. A., Frankenberg, C., Deutscher, N. M., Schneider, M., Barthlott, S., Blumenstock, T., Garcia, O. E., Hase, F., Jones, N., Mahieu, E., Notholt, J., Velazco, V., Landgraf, J., and Aben, I.: Validation of SCIAMACHY HDO/H_2O measurements using the TCCON and NDACC-MUSICA networks, Atmos. Meas. Tech., 8, 1799–1818, doi:10.5194/amt-8-1799-2015, 2015.

Schmid, B., Tomlinson, J. M., Hubbe, J. M., Comstock, J. M., Mei, F., Chand, D., Pekour, M. S., Kluzek, C. D., Andrews, E., Biraud, S. C., and McFarquhar, G. M.: The DOE ARM Aerial Facility, B. Am. Meteorol. Soc., 95, 723–742, doi:10.1175/BAMS-D-13-00040.1, 2014.

Schneising, O., Bergamaschi, P., Bovensmann, H., Buchwitz, M., Burrows, J. P., Deutscher, N. M., Griffith, D. W. T., Heymann, J., Macatangay, R., Messerschmidt, J., Notholt, J., Rettinger, M., Reuter, M., Sussmann, R., Velazco, V. A., Warneke, T., Wennberg, P. O., and Wunch, D.: Atmospheric greenhouse gases retrieved from SCIAMACHY: comparison to ground-based FTS measurements and model results, Atmos. Chem. Phys., 12, 1527–1540, doi:10.5194/acp-12-1527-2012, 2012.

Schneising, O., Heymann, J., Buchwitz, M., Reuter, M., Bovensmann, H., and Burrows, J. P.: Anthropogenic carbon dioxide source areas observed from space: assessment of regional enhancements and trends, Atmos. Chem. Phys., 13, 2445–2454, doi:10.5194/acp-13-2445-2013, 2013.

Sweeney, C., Karion, A., Wolter, S., Newberger, T., Guenther, D., Higgs, J. A., Andrews, A. E., Lang, P. M., Neff, D., Dlugokencky, E., Miller, J. B., Montzka, S. A., Miller, B. R., Masarie, K. A., Biraud, S., C., Novelli, P. C., Crotwell, M., Crotwell, A. M., Thoning, K., and Tans, P. P.: Seasonal climatology of CO_2 across North America from aircraft measurements in the NOAA/ESRL Global Greenhouse Gas Reference Network, J. Geophys. Res., 120, 5155–5190, doi:10.1002/2014JD022591, 2015.

Takagi, H., Saeki, T., Oda, T., Saito, M., Valsala, V., Belikov, D., Saito, R., Yoshida, Y., Morino, I., Uchino, O., Andres, R. J., Yokota T., and Maksyutov, S.: On the Benefit of GOSAT Observations to the Estimation of Regional CO_2 Fluxes, Sci. Online Lett. Atmos. (SOLA), 7, 161–164, doi:10.2151/sola.2011-041, 2011.

Tanaka, T., Miyamoto, Y., Morino, I., Machida, T., Nagahama, T., Sawa, Y., Matsueda, H., Wunch, D., Kawakami, S., and Uchino, O.: Aircraft measurements of carbon dioxide and methane for the calibration of ground-based high-resolution Fourier Transform Spectrometers and a comparison to GOSAT data measured over Tsukuba and Moshiri, Atmos. Meas. Tech., 5, 2003–2012, doi:10.5194/amt-5-2003-2012, 2012.

Tsuboi, K., Matsueda, H., Sawa, Y., Niwa, Y., Nakamura, M., Kuboike, D., Saito, K., Ohmori, H., Iwatsubo, S., Nishi, H., Hanamiya, Y., Tsuji, K., and Baba, Y.: Evaluation of a new JMA aircraft flask sampling system and laboratory trace gas analysis system, Atmos. Meas. Tech., 6, 1257–1270, doi:10.5194/amt-6-1257-2013, 2013.

Uchino, O., Kikuchi, N., Sakai, T., Morino, I., Yoshida, Y., Nagai, T., Shimizu, A., Shibata, T., Yamazaki, A., Uchiyama, A., Kikuchi, N., Oshchepkov, S., Bril, A., and Yokota, T.: Influence of aerosols and thin cirrus clouds on the GOSAT-observed CO_2: a case study over Tsukuba, Atmos. Chem. Phys., 12, 3393–3404, doi:10.5194/acp-12-3393-2012, 2012.

WMO: WMO Greenhouse Gas Bulletin, The State of Greenhouse Gases in the Atmosphere Using Global Observations through 2007, No. 4, World Meteorological Organization, available at: http://www.wmo.int/pages/prog/arep/gaw/ghg/GHGbulletin.html (last access: January 2015), 2008

WMO: WMO Greenhouse Gas Bulletin, The State of Greenhouse Gases in the Atmosphere Based on Global Observations through 2013, No. 10, World Meteorological Organization, available at: http://www.wmo.int/pages/prog/arep/gaw/ghg/GHGbulletin.html (last access: January 2015), 2014

Wofsy, S. C. and the HIPPO Science Team and Cooperating Modellers and Satellite Teams: HIAPER Pole-to-Pole Observations (HIPPO): fine-grained, global-scale measurements of climatically important atmospheric gases and aerosols, Philos. T. Roy. Soc. A, 369, 2073–2086, doi:10.1098/rsta.2010.0313, 2011.

Wofsy, S. C., Daube, B. C., Jimenez, R., Kort, E., Pittman, J. V., Park, S., Commane, R., Xiang, B., Santoni, G., Jacob, D., Fisher, J., Pickett-Heaps, C., Wang, H., Wecht, K., Wang, Q.-Q., Stephens, B. B., Shertz, S., Watt, A. S., Romashkin, P., Campos, T., Haggerty, J., Cooper, W. A., Rogers, D., Beaton, S., Hendershot, R., Elkins, J. W., Fahey, D. W., Gao, R. S., Moore, F., Montzka, S. A., Schwarz, J. P., Perring, A. E., Hurst, D., Miller, B. R., Sweeney, C., Oltmans, S., Nance, D., Hintsa, E., Dutton, G., Watts, L. A., Spackman, J. R., Rosenlof, K. H., Ray, E. A., Hall, B., Zondlo, M. A., Diao, M., Keeling, R., Bent, J., Atlas, E. L., Lueb, R., and Mahoney, M. J.: HIPPO merged 10-second Meteorology, Atmospheric Chemistry, Aerosol Data (R_20121129), used data file "HIPPO_all_missions_merged_10s_20121129.tbl", Carbon Dioxide Information Analysis Center, Oak Ridge National Laboratory, Oak Ridge, Tennessee, USA, available at: http://dx.doi.org/10.3334/CDIAC/hippo_010 (last access: July 2013), 2012.

Wunch, D., Wennberg, P. O., Toon, G. C., Keppel-Aleks, G., and Yavin, Y. G.: Emissions of greenhouse gases from a

North American megacity, Geophys. Res. Lett., 36, L15810, doi:10.1029/2009GL039825, 2009.

Wunch, D., Toon, G. C., Wennberg, P. O., Wofsy, S. C., Stephens, B. B., Fischer, M. L., Uchino, O., Abshire, J. B., Bernath, P., Biraud, S. C., Blavier, J.-F. L., Boone, C., Bowman, K. P., Browell, E. V., Campos, T., Connor, B. J., Daube, B. C., Deutscher, N. M., Diao, M., Elkins, J. W., Gerbig, C., Gottlieb, E., Griffith, D. W. T., Hurst, D. F., Jiménez, R., Keppel-Aleks, G., Kort, E. A., Macatangay, R., Machida, T., Matsueda, H., Moore, F., Morino, I., Park, S., Robinson, J., Roehl, C. M., Sawa, Y., Sherlock, V., Sweeney, C., Tanaka, T., and Zondlo, M. A.: Calibration of the Total Carbon Column Observing Network using aircraft profile data, Atmos. Meas. Tech., 3, 1351–1362, doi:10.5194/amt-3-1351-2010, 2010.

Wunch, D., Toon, G. C., Blavier, J.-F. L., Washenfelder, R. A., Notholt, J., Connor, B. J., Griffith, D. W. T., Sherlock, V., and Wennberg, P. O.: The Total Carbon Column Observing Network, Phil. Trans. R. Soc. A, 369, 2087–2112, doi:10.1098/rsta.2010.0240, 2011a.

Wunch, D., Wennberg, P. O., Toon, G. C., Connor, B. J., Fisher, B., Osterman, G. B., Frankenberg, C., Mandrake, L., O'Dell, C., Ahonen, P., Biraud, S. C., Castano, R., Cressie, N., Crisp, D., Deutscher, N. M., Eldering, A., Fisher, M. L., Griffith, D. W. T., Gunson, M., Heikkinen, P., Keppel-Aleks, G., Kyrö, E., Lindenmaier, R., Macatangay, R., Mendonca, J., Messerschmidt, J., Miller, C. E., Morino, I., Notholt, J., Oyafuso, F. A., Rettinger, M., Robinson, J., Roehl, C. M., Salawitch, R. J., Sherlock, V., Strong, K., Sussmann, R., Tanaka, T., Thompson, D. R., Uchino, O., Warneke, T., and Wofsy, S. C.: A method for evaluating bias in global measurements of CO_2 total columns from space, Atmos. Chem. Phys., 11, 12317–12337, doi:10.5194/acp-11-12317-2011, 2011b.

Wunch, D., Toon, G. C., Sherlock, V., Deutscher, N. M., Liu, X., Feist, D. G., and Wennberg, P. O.: The Total Carbon Column Observing Network's GGG2014 Data Version. Carbon Dioxide Information Analysis Center, Oak Ridge National Laboratory, Oak Ridge, Tennessee, USA doi:10.14291/tccon.ggg2014.documentation.R0/1221662, 2015.

Xiong, X., Barnet, C., Maddy, E., Sweeney, C., Liu, X., Zhou, L., and Goldberg, M.: Characterization and validation of methane products from the Atmospheric Infrared Sounder (AIRS), J. Geophys. Res., 113, G00A01, doi:10.1029/2007JG000500, 2008.

Yokota, T., Yoshida, Y., Eguchi, N., Ota, Y., Tanaka, T., Watanabe, H., and Maksyutov, S.: Global Concentrations of CO_2 and CH_4 Retrieved from GOSAT: First Preliminary Results, Sci. Online Lett. Atmos. (SOLA), 5, 160–163, doi:10.2151/sola.2009-041, 2009.

Yoshida, Y., Ota, Y., Eguchi, N., Kikuchi, N., Nobuta, K., Tran, H., Morino, I., and Yokota, T.: Retrieval algorithm for CO_2 and CH_4 column abundances from short-wavelength infrared spectral observations by the Greenhouse gases observing satellite, Atmos. Meas. Tech., 4, 717–734, doi:10.5194/amt-4-717-2011, 2011.

Yoshida, Y., Kikuchi, N., Morino, I., Uchino, O., Oshchepkov, S., Bril, A., Saeki, T., Schutgens, N., Toon, G. C., Wunch, D., Roehl, C. M., Wennberg, P. O., Griffith, D. W. T., Deutscher, N. M., Warneke, T., Notholt, J., Robinson, J., Sherlock, V., Connor, B., Rettinger, M., Sussmann, R., Ahonen, P., Heikkinen, P., Kyrö, E., Mendonca, J., Strong, K., Hase, F., Dohe, S., and Yokota, T.: Improvement of the retrieval algorithm for GOSAT SWIR XCO_2 and XCH_4 and their validation using TCCON data, Atmos. Meas. Tech., 6, 1533–1547, doi:10.5194/amt-6-1533-2013, 2013.

Zhou, M., Dils, B., Wang, P., Detmers, R., Yoshida, Y., O'Dell, C. W., Feist, D. G., Velazco, V. A., Schneider, M., and De Mazière, M.: Validation of TANSO-FTS/GOSAT XCO_2 and XCH_4 glint mode retrievals using TCCON data from near-ocean sites, Atmos. Meas. Tech., 9, 1415–1430, doi:10.5194/amt-9-1415-2016, 2016.